PHOTONIC SENSORS / Vol. 13, No. 4, 2023: 230419

MEMS and MOEMS Gyroscopes: A Review

Wenyi HUANG[1], Xing YAN[1], Sengyu ZHANG[1], Zhe LI[2], Jamal N. A. HASSAN[1], Dingwei CHEN[1], Guangjun WEN[1], Kai CHEN[2], Guangwei DENG[3], and Yongjun HUANG[1*]

[1]*School of Information and Communication Engineering, Sichuan Provincial Engineering Research Center of Communication Technology for Intelligent IoT, University of Electronic Science and Technology of China, Chengdu 611731, China*

[2]*School of Automation Engineering, University of Electronic Science and Technology of China, Chengdu 611731, China*

[3]*Institute of Fundamental and Frontier Sciences, University of Electronic Science and Technology of China, Chengdu 610054, China*

[*]Corresponding author: Yongjun HUANG E-mail: yongjunh@uestc.edu.cn

Abstract: Micro-gyroscopes using micro-electro-mechanical system (MEMS) and micro-opto-electro-mechanical system (MOEMS) are the new-generation and recently well-developed gyroscopes produced by the combinations of the traditional gyroscope technology and MEMS/MOEMS technologies. According to the working principle and used materials, the newly-reported micro-gyroscopes in recent years include the silicon-based micromechanical vibratory gyroscope, hemispherical resonant gyroscope, piezoelectric vibratory gyroscope, suspended rotor gyroscope, microfluidic gyroscope, optical gyroscope, and atomic gyroscope. According to different sensitive structures, the silicon-based micromechanical vibratory gyroscope can also be divided into double frame type, tuning fork type, vibrating ring type, and nested ring type. For those micro-gyroscopes, in recent years, many emerging techniques are proposed and developed to enhance different aspects of performances, such as the sensitivity, angle random walk (ARW), bias instability (BI), and bandwidth. Therefore, this paper will firstly review the main performances and applications of those newly-developed MEMS/MOEMS gyroscopes, then comprehensively summarize and analyze the latest research progress of the micro-gyroscopes mentioned above, and finally discuss the future development trends of MEMS/MOEMS gyroscopes.

Keywords: Micro-gyroscope; MEMS; MOEMS; angular random walk; bias instability

Citation: Wenyi HUANG, Xing YAN, Sengyu ZHANG, Zhe LI, Jamal N. A. HASSAN, Dingwei CHEN, *et al.*, "MEMS and MOEMS Gyroscopes: A Review," *Photonic Sensors*, 2023, 13(4): 230419.

1. Introduction

As a device for measuring the angular rate of moving objects, the gyroscope is widely used in civil and military areas, such as aerospace, automobile, consumer electronics, ship navigation, and guided ammunition [1–5]. Motivated by high performance large-scale gyroscopes, with the emergences and developments of micro-electro-mechanical system (MEMS) and micro-opto-electro-mechanical system (MOEMS) technologies, a new generation of the micro-gyroscope based on such MEMS/MOEMS technologies has become one of the focused

Received: 15 December 2022 / Revised: 6 June 2023

DOI: 10.1007/s13320-023-0693-x
Article type: Review

development directions in the academic and industrial areas [6–9]. MEMS/MOEMS gyroscopes have developed rapidly since the Draper Laboratory produced the first non-rotor silicon micromechanical gyroscopes in 1988 [10]. In the past several years, with the continuous developments of MEMS/MOEMS processing technologies, the performances of silicon MEMS/MOEMS gyroscopes based on different principles, structures, and materials have been greatly improved, mainly including the mechanical micro-gyroscopes based on Coriolis principles or angular momentum conservation, and optical gyroscopes based on the Sagnac effect. The previous reported reviews [2, 3, 6–10], however, only focused on the traditional MEMS gyroscopes and there is no discussion on the emerging MOEMS gyroscopes. Therefore, this review paper will summarize the latest research progress of MEMS/MOEMS gyroscopes and discuss some development trends.

2. Main performance indexes of micro-gyroscope

Before the progress analysis on micro-gyroscopes, the main performance indexes, including the bias instability (BI), angular random walk (ARW), scale factor (SF), dynamic measurement range, bandwidth, and anti-interference, should be clarified according to the different application environments [11–15]. Specifically, the two most important parameters for the inertial navigation applications are the BI and ARW. The BI represents the accuracy of the gyroscope for a long time, which reflects the change of the bias with time after the gyroscope is electrically stabilized, related to the flicker noise. And the ARW represents the accuracy of the gyroscope in a relatively short time, related to the thermo-mechanical white noise, which results in a zero-mean error with a standard deviation. Besides, the SF, also named sensitivity, is the linear correlation coefficient between the output and input angular rate. A large SF can suppress the noise and interference to achieve a higher signal-to-noise ratio (SNR). Improving the mechanical quality factor can increase the SF, but it also results in a smaller bandwidth. Moreover, in general, a gyroscope with the proper dynamic measurement range (or full-scale range) is selected because the relative accuracy of a sensor is constant; theoretically the better ARW and larger SF will result in the smaller dynamic measurement range. That means that not all the performance indexes can be improved at the same time, and generally the researchers need to find a trade-off point based on different application requirements. On the other hand, although the gyroscope is a sensor that measures the angular rate and angular vibration, too much impact from the outside will cause it to fail. For example, one parameter named the shock range means the largest acceleration range bearable by the gyroscope.

According to the key parameters mentioned above, gyroscopes can be generally divided into three grades: rate-grade, tactical-grade, and inertial-grade, which correspond to low precision, medium precision, and high precision performances, respectively. Specifically, the rate-grade gyroscopes are mainly used in the consumer electronics, automobile navigation, and other occasions. And tactical-grade gyroscopes are mainly used in the aircraft navigation, attitude positioning, and other fields, which require both short-term and long-term accuracies. Moreover, inertial-grade gyroscopes are often used in the navigation, satellite positioning, scientific survey, and other fields, which require the ultra-high precision. The conventional definitions of performance indexes for different levels of these micro-gyroscopes can be referred to Table 1 [16].

Generally, MEMS/MOEMS gyroscopes can be divided into electrostatic driving [17], piezoelectric driving [18], and electromagnetic driving [19], in terms of the driving methods; and can be divided into capacitance sensing [20], current sensing [21], resistance sensing [22], frequency sensing [9], and tunnel effect sensing [23], in terms of the sensing methods; and also can be divided into vibration type [24] and rotor type [25], from the structure difference. The vibration-type silicon micro-gyroscope can also be further divided into linear vibration [26] and angular vibration [27]. More specifically, according to the principles and sensitive structure, the vibration-type silicon micro-gyroscope can be divided into the double frame type [28–41], tuning fork type [42–70], micro-hemisphere resonance type [71–86], vibration ring type [87–94], nested ring [95–116], piezoelectric vibration type [117–129], suspended rotor type [130–136], optical gyroscope [137–149], and atomic gyroscope [150–166], as shown in Fig. 1.

Table 1 Performance index range of micro-gyroscopes with different precisions [16].

Parameters	Rate-grade	Tactical-grade	Inertial-grade
Bias instability (°/h)	10–1 000	0.1–10	<0.01
ARW (°/h$^{1/2}$)	>0.5	0.5–0.05	<0.01
Scale factor (%)	0.1–1	0.01–0.1	<0.001
Bandwidth (Hz)	>70	100	100
Full scale range (°/s)	50–1 000	>500	>400
Shock range [*g* (N/kg)]	10^3	10^3–10^4	10^3

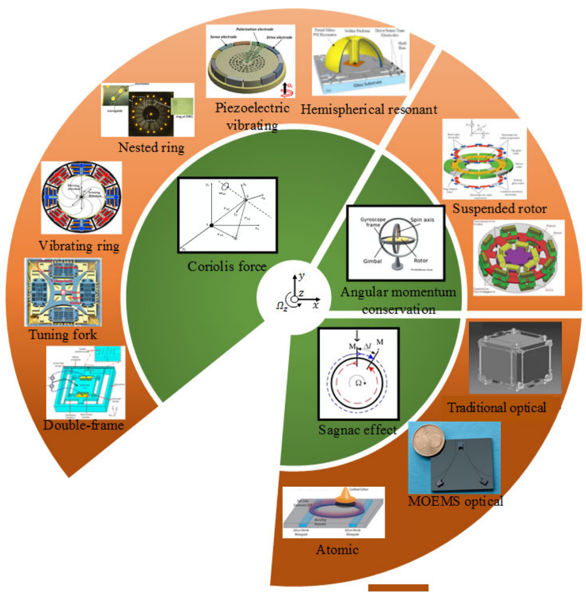

Fig. 1 Summary of MEMS/MOEMS gyroscope classifications.

3. Research progress of MEMS mechanical gyroscopes

The MEMS/MOEMS mechanical gyroscope is mainly based on the Coriolis effect to measure the angular rate or vibration [8, 9], including the double frame type, tuning fork type, micro-hemisphere resonance type, vibration ring type, nested ring type, and piezoelectric vibration type. The simplest geometry structure consists of a mass, which is driven to vibrate along a drive axis and secondarily vibrate along the perpendicular sense axis due to the Coriolis effect, as shown in Fig. 2(a) [167]. In a coordinate system rotating at an angular rate ω, a mass m vibrating (or moving) with a velocity v experiences a Coriolis force:

$$\mathbf{F}_C = -2m(\boldsymbol{\omega}\times\mathbf{v}) .$$

Specifically, the angular rate or vibration acting on the MEMS gyroscope is converted into the displacement of the test mass of the sensitive structure based on the Coriolis effect. Then, the sensed displacement is converted into the output electrical signal through the transducer structure. Finally, the angular rate or vibration can be calculated through the corresponding signal processing circuit. Besides, the MEMS/MOEMS mechanical gyroscopes work in a similar way as the traditional conventional gyroscope to directly measure orientation instead of the angular rate based on the angular momentum conservation principle, as shown in Fig. 2(b) [167], such as the suspended rotor micro-gyroscope. The conservation of angular momentum leads to the wheel resisting the orientation changes, and then the angles between adjacent gimbals will change and can be measured by angle pick-offs.

3.1 Double-frame micro-gyroscope

3.1.1 Double-frame MEMS micro-gyroscope

The double-frame micro-gyroscope is usually a single sensitive test mass, which can be divided into the un-decoupled structure [28–30], single-decoupled structure [31–37], and double-decoupled structure [38–41] according to whether it is decoupled between the drive mode and sense mode. In 1991, P. Greiff *et al.* [28] from the Draper Laboratory produced the first non-rotor silicon dual-frame micro-gyroscope sample. The driving plate drives the outer frame by the electrostatic force at a constant amplitude, and the vibration is transmitted into the inner frame by the rigid connecting shaft, making the inner and outer frames vibrate along the driving axis at the same frequency. When an angular rate is given along the rotation axis, due to the Coriolis force, the sensing mass located in the central squeezes the sensitive electrode plate, and then the amplitude of the internal frame is detected by measuring the change of the electrode capacitance. The sensing noise limit for such kind of gyroscope is 4 °/s/Hz$^{1/2}$ at the 1-Hz bandwidth, corresponding to the ARW of 240 °/h$^{1/2}$.

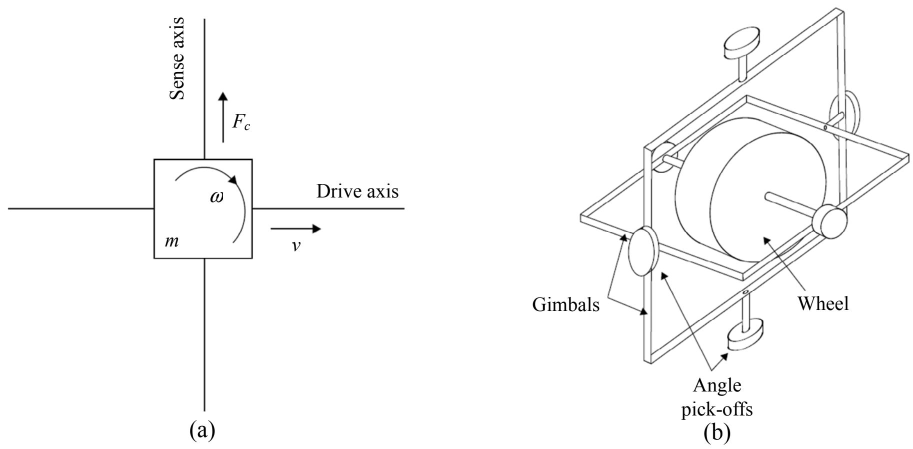

Fig. 2 Vibrating mass gyroscope (a) and a conventional mechanical gyroscope (b) [167].

Based on the firstly reported micro-gyroscope in 2000, S. E. Alper [29] proposed a dual-frame gyroscope based on the standard three-layer polysilicon surface micro-machining technology, and its structure is shown in Fig. 3(a). The gyroscope provides larger driving and sensing capacitance output values to improve the sensitivity, and the resonant frequencies of the driving and sensing modes to be controlled by the electrostatic force. When the frequency mismatch between the two modes is 4.65%, the circuit can detect a change of 0.1 fF, and the sensitivity is up to 45 mV/fF. In 2005, K. Maenaka, *et al.* [30] proposed a new double-circular and dual-frame gyroscope, with two independent coils attached to its internal and external frames, which were vertically supported by two torsion rods, as shown in Fig. 3(b). The resolution of this gyroscope is 0.264 °/h$^{1/2}$ and 38.4 °/h$^{1/2}$ at 1-kHz and 0.1-kHz bandwidths, respectively.

3.1.2 Double-frame MOEMS micro-gyroscope

Based on the MOEMS techniques, in 2002, M. Norgia *et al.* [31] firstly reported a single-mass measuring block frame-type gyroscope by using the optical fiber sensing method. However, it is not well integrated. In 2018, A. Sheikhaleh *et al.* [32] proposed a frame-type gyroscope with electrostatic driving and photonic crystal sensing, as shown in Fig. 3(c). However, only simulation results show that the structure has a working bandwidth of 200 Hz, a mechanical sensitivity $\Delta y/\Delta \Omega$ of 0.14 nm/(°/s), an optical sensitivity $\Delta\lambda/\Delta\Omega$ of 0.051 nm/(°/s), and a measurement range of ±500 °/s.

On another hand, in 2016, C. Trigona, *et al.* [33, 34] reported a frame-type MOEMS gyroscope with the electrostatic drive and PBG material output to detect the sensing displacement, as shown in Fig. 3(d). The comb capacitor driver makes the mass block resonate in the vertical direction. Under the condition of the applied angular rate, the mass block is shifted in the horizontal direction, so that the air gap of the photonic bandgap (PBG) material is changed. This change in the air gap could be detected through a subsequent change in the optical refraction spectrum, which could be measured through integrated photonic detectors. The sensitivity of this gyroscope is 18.7 mV/°/s. In 2021, M. Li *et al*. [35, 36] and K. Xie *et al*. [37] also reported a frame-type MOEMS gyroscope with electromagnetic driving and grating sensing, as shown in Fig. 3(e). The gyroscope's proof mass is placed in a uniform magnetic field produced by the permanent magnets and is driven into resonance in the x direction by the electrical magnetic field. The induced displacement in the z axis is changed into the light intensity of the grating sensing structure. From the experimental demonstration, its optical sensitivity could reach 0.09 %/nm.

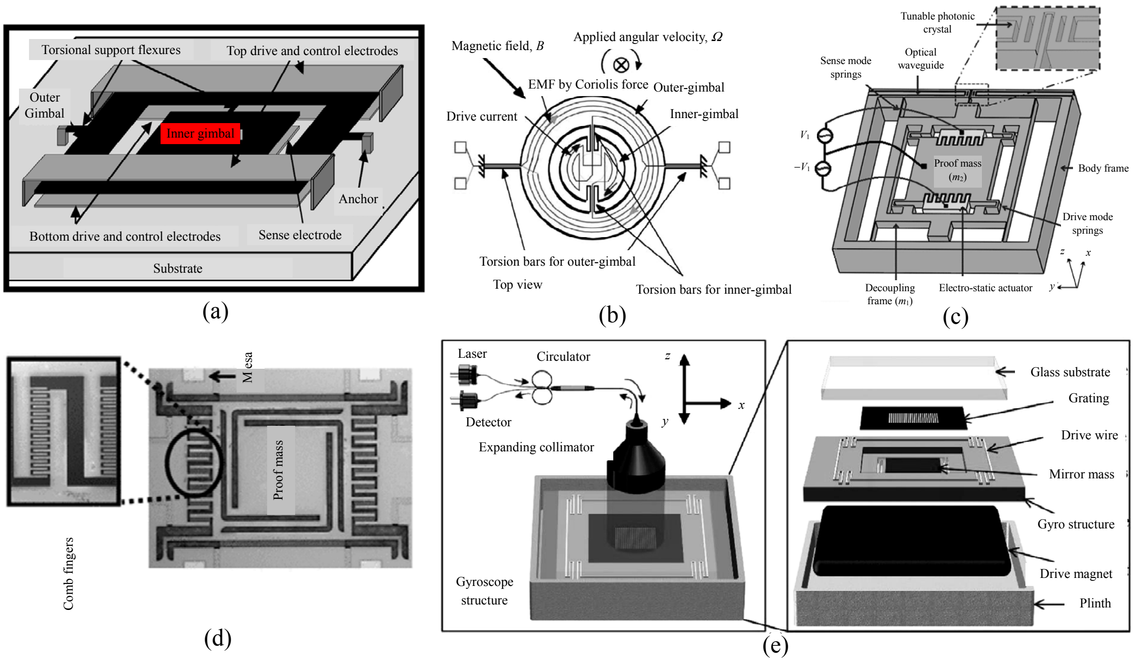

Fig. 3 Double-frame MEMS/MOEMS gyroscopes [29, 30, 32–37].

As the first type of the MEMS/MOEMS gyroscope made by the Coriolis force principle, the double-frame structure has a simple configuration, small package size, and no rotor structure, which is suitable for low precision applications. The main factors affecting the accuracy of this kind of gyroscope are the resonance amplitude limit of the test mass in the driving direction and the sensing capacity of the transducer structure. Therefore, it is necessary to design the connecting structure of the test mass to improve the amplitude of driving and sensing modes and the sensing ability of the transducer structure.

3.2 Tuning fork micro-gyroscope

The tuning fork gyroscope is the most widely studied type of the micro-gyroscope in recent years. According to the number of the test mass, it can be mainly divided into dual-test-mass and four-test-mass structures.

3.2.1 Dual-test-mass tuning fork gyroscope

Taking the tuning fork gyroscope with the first dual-test-mass configuration manufactured by the Draper Laboratory in 1993, as an example, its structure is shown in Fig. 4(a) [42]. The dual-test-mass and differential capacitor structure greatly improves the sensitivity of the gyroscope. The resolution of such a gyroscope at the 1-Hz bandwidth is 0.19 °/s/Hz$^{1/2}$, the ARW is 0.72 °/h$^{1/2}$, and the BI is 55 °/h. In 1998, M. Lutz *et al*. [43] proposed another kind of tuning fork gyroscope with the dual-test-mass structure using the silicon micromechanical accelerometer to measure the output, as shown in Fig. 4(b). It consists of a permanent magnet, two test-mass, and two independent accelerometers. When an angular rate is applied to the structure, the two accelerometers will sense the magnitude of the Coriolis force. The sensitivity of this gyroscope is 18 mV/°/s, and the resolution is 1.2 °/h$^{1/2}$ at the 100-Hz bandwidth.

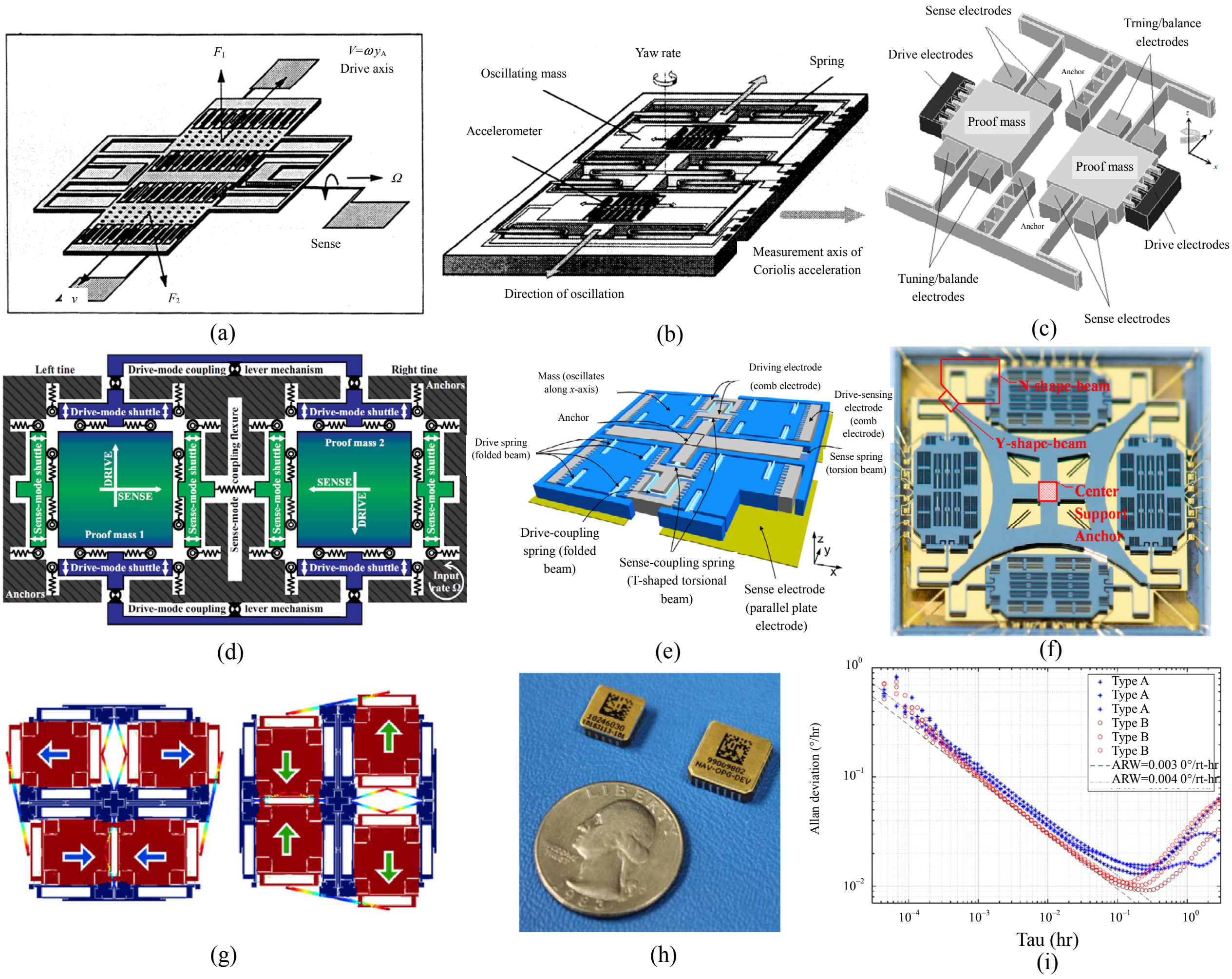

(a) (b) (c) (d) (e) (f) (g) (h) (i)

Fig. 4 Tuning fork micro-gyroscopes [42, 43–52, 69, 70].

In recent years, A. Sharma *et al*. [44–48] proposed a high quality factor (Q-factor) tuning fork gyroscope based on the silicon-on-insulator (SOI) process, as shown in Fig. 4(c). Its Q-factors for the driving mode and sensing mode are 8.1×10^4 and 6.4×10^4, and the high Q-factors contribute to the high resolution. As a result, at the 12-Hz bandwidth, its sensitivity is 1.25 mV/°/s and resolution is 0.01 °/s/Hz$^{1/2}$. In 2009, they also reported a modified tuning fork gyroscope with a better performance [48], whose maximum sensitivity was 88 mV/°/s, the ARW was 0.003 °/h$^{1/2}$, and the BI was better than 0.15 °/h. In 2007–2009, a multi-degree-of-freedom tuning fork micro-gyroscope was reported, as shown in Fig. 4(d) [49–51]. This gyroscope is coupled with the left and right test masses in the driving direction through an elastic beam, and its sensing mode is a two-degree-of-freedom system. The sensitivity of this gyroscope is 7.68 μV/°/s.

3.2.2 Four-test-mass tuning fork gyroscope

The four-test-mass gyroscope consists of four identical single test masses, which can also be regarded as two dual-test-mass tuning fork gyroscopes. In 2012, a four-test-mass tuning fork micro-gyroscope was reported [52], as shown in Fig. 4(e). In the driving direction, two test masses of each tuning fork are coupled together by an elastic beam. Meanwhile, the two test masses of each tuning fork are coupled together through the frame structure in the sensing direction. The gyroscope operates at a mode mismatch of 5 Hz with an ARW of 26.4 °/$h^{1/2}$.

Quite recently, researchers have conducted a lot of researches on tuning fork gyroscopes and developed various tuning fork micro-gyroscopes [53–68], such as the *z*-axis four-test-mass micro-gyroscope reported in 2016, as shown in Fig. 4(f) [67, 68]. The four test masses of the gyroscope are coupled together through different types of beam configurations. The left and right test masses and the upper and lower test-masses form two tuning fork structures, respectively. The gyroscope has a central frequency of 6.8 kHz and a quality factor greater than 8 000 at a pressure of 30 Pa. The white noise level or ARW of the gyroscope is 43.11 °/$h^{1/2}$ and the BI is 0.12 °/h. And in the same year, the researchers presented a silicon MEMS quadruple mass gyroscope with an interchangeable whole angle, self-calibration, and force rebalance mechanizations. The gyroscope without a getter with a quality factor of 1×10^3 reveals an ARW of 1.2 °/$h^{1/2}$. And the gyroscope with a getter with a quality factor of 1×10^6 show a better ARW of 0.06 °/$h^{1/2}$. The finite element modeling for the quad mass gyroscope resonator show the two mode-shapes characteristics in Fig. 4(g) [69].

In 2019, the researchers in Honeywell reported an MEMS out-plane gyroscope suitable for platform stabilization with an ultra-high performance, fabricated by a similar process to the tactical-grade gyroscope. Honeywell fabricated the MEMS gyroscope in a 20-pin package used in HG1930 IMU and in 28-pin in this paper shown in the upper right of Fig. 4(h). It has achieved the ARW of 0.36 °/$h^{1/2}$, median bias stabilities over the temperature of 0.2 °/h–0.12 °/h, and the bandwidth greater than 300 Hz. And in Fig. 4(i), the Allan deviation analysis of 25 ℃ bias measurement is taken at 12.5 Hz [70].

Due to their multiple-test-mass structures, the tuning fork gyroscopes can distinguish the displacement of the sensing direction caused by the Coriolis force from that caused by the linear impact interference, such as the linear acceleration through the structure of the double test mass, thus making the MEMS gyroscope has the possibility of the practical application. However, the tuning fork structure needs to be decoupled to reduce the coupling displacement of driving and sensing modes, and requires two identical test masses, which makes it harder to the MEMS machining technology and restricts the precision and performance of such kind of gyroscopes.

3.3 Hemisphere/vibrating ring micro-gyroscope

The hemisphere and vibrating ring gyroscopes are mainly composed of the resonant structure and control circuit, which use two orthogonal modes of resonator vibration, as shown in Fig. 5, to sense the angular rate based on the Coriolis force. Because of the high symmetry of the resonant structure, the hemisphere and vibrating gyroscopes have very similar nature of the two modes and the strong resistance to the random vibration due to the temperature change and other non-ideal factors. Therefore, it can theoretically achieve the better performance than the previously discussed tuning fork gyroscope. The vibration is distributed on the resonator and has four wave belly points and four wave nodes, which is called the driving mode. Another sensing mode is 45° different from the driving mode, and its wave belly point is just the wave node of the driving mode, and the two vibration modes are orthogonal to each other. Under ideal conditions, the electrode located outside the resonator in the vertical direction drives the resonator to work in the driving mode, and the sensing mode has no vibration output. When the angular rate perpendicular to the resonator is applied, the energy is transferred from the driving mode to the sensing mode due to the Coriolis force. The sensitive electrode outside the resonator calculates the angular rate by detecting the vibration amplitude of the sensing mode.

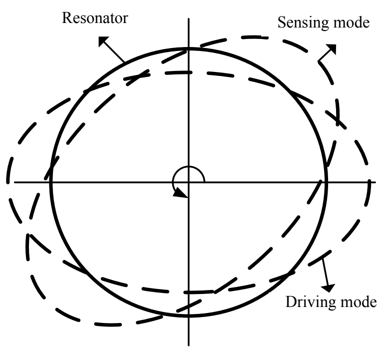

Fig. 5 Operating principle of the hemisphere/vibrating ring micro-gyroscope.

3.3.1 Micro-hemispherical resonant micro-gyroscope

The principle of this kind of gyroscope seems quite simple, but the main difficulty of its limited accuracy lies in the manufacture of the highly symmetrical and smooth hemispherical resonant structure with the high mechanical quality factor. In 2013, J. Cho *et al.* [71] reported a hemispherical resonant gyroscope prototype as shown in Fig. 6(a) with the BI of 1 °/h and ARW of 0.106 °/h$^{1/2}$. The anchor of the resonant is self-aligned to the rest of the structure to fabricate a birdbath resonator with a good structure. Subsequently, prototypes with better parameters were reported in 2015, 2017, and 2020 [72–74]. The prototype in 2020 is shown in Fig. 6(b), with the BI of 0.027 °/h and ARW of 0.0062 °/h$^{1/2}$. In 2015, the researchers described a quality factor of over 1 million and a high-frequency symmetry of 132 ppm on both wineglass modes on a fused silica resonator at a compact size of 7 mm. They could enable batch-fabrication of high-performance fused silica wineglass gyroscopes on a wafer surface at a significantly lower cost than their precision-machined macro-scale counterparts shown in Fig. 6(c) [75–76].

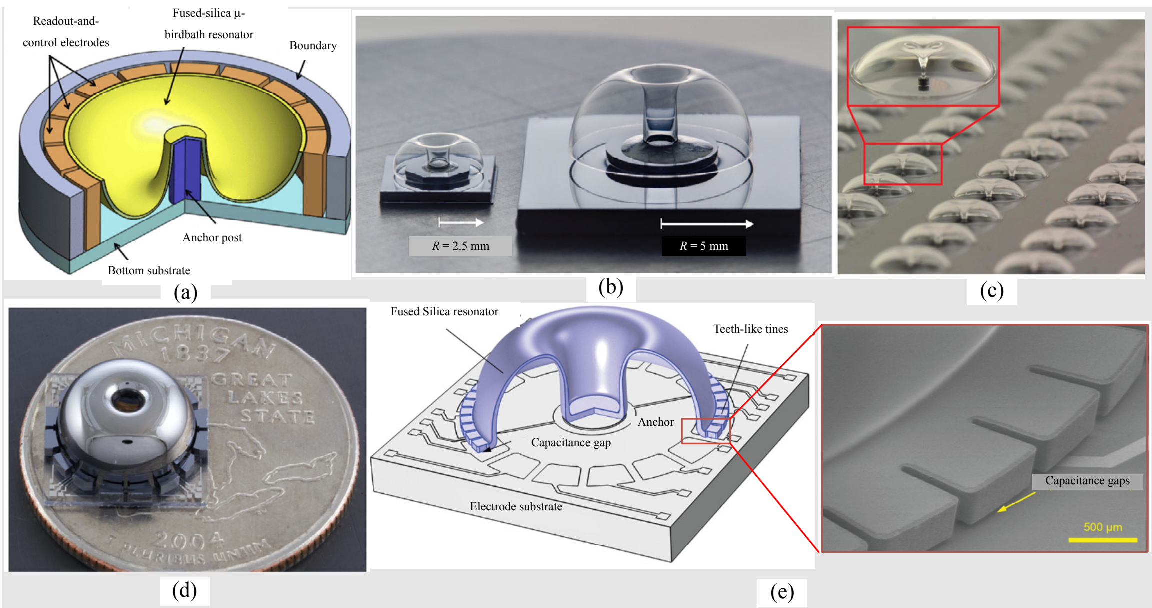

Fig. 6 Micro-hemispherical resonant micro-gyroscope [71–79].

In 2020, the researchers from University of Michigan reported a record-high performance from a fused-silica micro precision shell integrating (PSI) gyroscope shown in Fig. 6(d), which had an ARW of 0.000 16 °/h$^{1/2}$ and a short-term BI of 0.001 4 °/h without temperature compensation. And a fused silica of the PSI gyroscope has achieved a mechanical quality factor of 5.2 million with a diameter of 1 cm. It has the better performance with such a small scale than the micro hemispherical resonator gyroscope (micro-HRG) reported previously. And they improved the quality factor of the micro birdbath resonator to 8.7 million at 5.897 kHz and 12.5 million at 12.798 kHz in 2021 [77, 78].

In 2021, the rate-integrating micro-hemispherical resonator micro-gyroscope with the structure as shown in Fig. 6(e) was produced by B. Li, *et al.* [79–86] in China. The contact edge has 16 T-shaped test masses to increase the contact area with the surface electrode to improve the sensitivity. The resonance structure is processed by the high-temperature rotary blowing technology. Moreover, femtosecond laser etching is used to achieve frequency matching modification with the accuracy within 0.1 Hz. The frequency difference is 49 MHz, the BI is 0.235 °/h, and the ARW is 0.006 6 °/h$^{1/2}$.

The hemispherical resonant gyroscope with the high measuring accuracy, strong stability, reliability, and long working life, is often used in the related equipment in the field of aerospace. However, because the resonance of the structure of the processing is difficult, expensive, and bulky against integration shortcomings, it is difficult to apply it to the low cost of the consumption area.

3.3.2 Vibrating ring micro-gyroscope

In order to reduce the processing difficulty of the hemispherical resonant gyroscope, the ring resonator attracted the attention of researchers in the field of the gyroscope. In 1994, M. W. Putty *et al.* [87] proposed the first vibrating ring gyroscope as shown in Fig. 7(a), which consists of one vibrating ring, eight elastically supported suspension beams, one driving electrode, one sensitive electrode, and one control circuit. In 2001, F. Ayazi *et al.* [88, 89] made a vibrating ring gyroscope sample with the similar structure [as shown in Fig. 7(a)] with the quality factor of 1 200, sensitivity of 200 μV/°/s, bandwidth of 1 Hz, and resolution of less than 60 °/h$^{1/2}$ in a low vacuum environment by using the high aspect ratio combined with the polycrystalline silicon and monocrystalline silicon micromechanical manufacturing technology (HARPSS). After the further improvement, a vibrating ring gyroscope with the quality factor of 1.2×10^4, sensitivity of 132 mV/°/s, and ARW of 0.173 °/h$^{1/2}$ is achieved [90]. In 2009, M. F. Zaman [91] manufactured a vibrating ring gyroscope with a star structure formed as a merged superposition of two square shells, yielding in-plane flexural modes that are utilized to sense the rotation along the normal axis, as shown in Fig. 7(b). In a vacuum environment, its sensitivity reaches 16.7 mV/°/s, the BI is 3.47 °/h, and the ARW is 0.09 °/h$^{1/2}$. The prototype is implemented with the 65-μm-thick trench-refilled polysilicon structural material by the HARPSS process.

In the beginning, the research on the vibratory ring gyroscope mainly focused on the theoretical analysis and simulation design. Until 2010, D. Chen *et al.* [92] developed a vibrating ring gyroscope with the design, fabrication, package, and test, which had the strong impact resistance (over 10 000 g), as shown in Fig. 7(c). This ring is electrostatically driven, capacitively sensed, and stiffness controlled using 16 electrode anchors inside the ring to achieve resonant frequent balancing. And the researchers also reported a new method to fabricate the vibrating ring gyroscope through simple all-silicon high aspect ratio microfabrication technologies with only 2 masks. Under vacuum conditions, the quality factor is about 2.2×10^4, the sensitivity is 1.5 mV/°/s, and the ARW is 3 °/h$^{1/2}$. In 2015, S. Yoon, *et al.* [93] designed an impact-resistant vibrating ring silicon micro-gyroscope, as shown in Fig. 7(d). There is a flexure, which is designed to absorb shocks effectively and minimize the shear stress and tangential displacement of the ring, when it is subjected to shocks. Its resonant frequency is 17 kHz, which could withstand 15 000 g of the impact force. The BI of this gyroscope is better than 1 °/h, the scale factor nonlinearity is better than 50 ppm, and the ARW is better than 1 °/h$^{1/2}$. And in 2020, Z. Li *et al.* [94] reported a vibratory ring gyroscope with different structures manufactured by the deep reactive ion etching technology, as shown in Fig. 7(e), with the ARW of 0.776 °/h$^{1/2}$ and BI of 8.86 °/h. And the reported structure achieved relatively high linearity by using the combination hinge and variable-area capacitance strategy instead of the conventional approach via variable-separation drive/sense strategy.

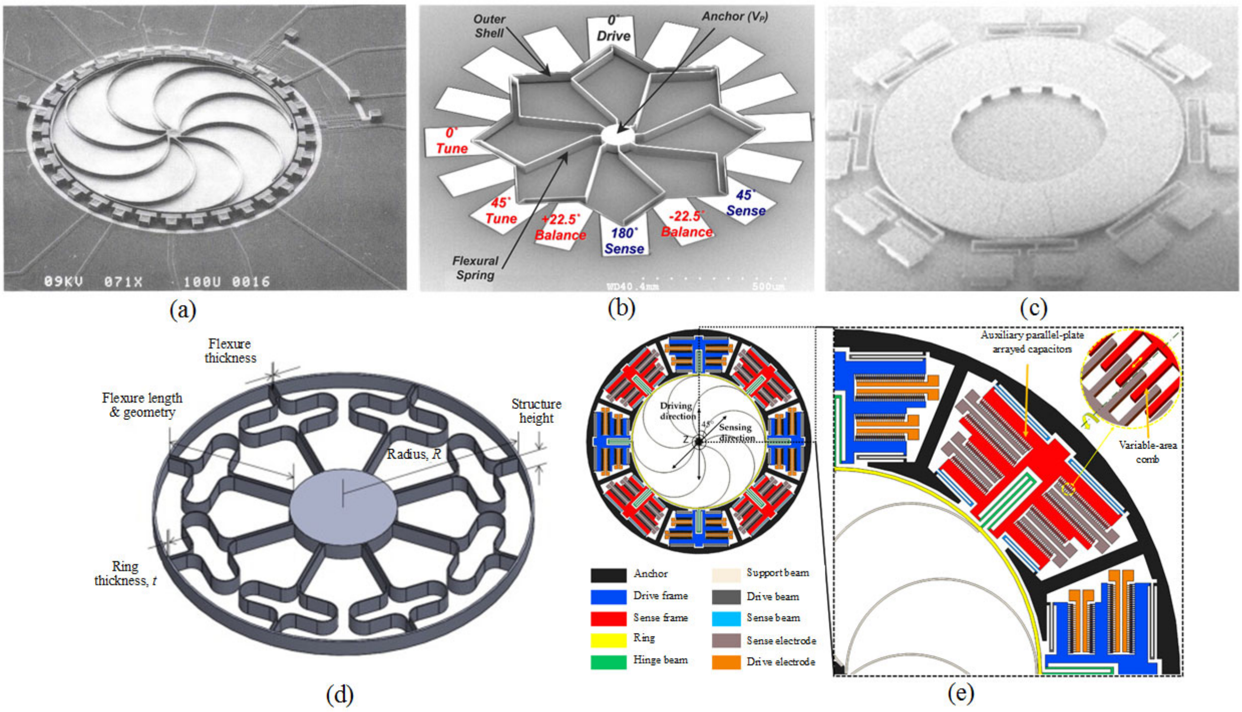

Fig. 7 Vibrating ring micro-gyroscope [87, 91, 92–94].

3.3.3 Nested ring micro-gyroscope

The vibration ring gyroscopes require a completely symmetrical structure, and the nonlinear dynamics of the vibration ring gyroscope is difficult to solve. And the high cost and complex nonlinear problems make the vibration ring gyroscope not widely manufactured. Moreover, the nested ring gyroscope is inherited and developed from the vibrating ring gyroscope and hemispherical resonant gyroscope. Based on the Coriolis force, the nested ring gyroscope is composed of multiple resonant rings with increasing radius as the sensitive structure and a large number of electrodes placed between the resonant rings. Compared with the vibrating-ring gyroscope, the circular symmetrical structure not only has the ability to resist the external impact interference, but also increases the mass of the sensitive structure through multiple resonance rings. Moreover, a large number of built-in electrodes improve the ability to drive the test-mass.

As early as 2003, Boeing Company and Jet Propulsion Laboratory proposed the nested ring gyroscope. In 2008, it was reported that the BI of the gyroscope could reach 0.25 °/h [95] and obtain 0.01 °/h contributed by its error compensation and temperature control in 2016 [96, 97], as shown in Fig. 8(a). And in 2009, a nested ring gyroscope based on the single crystal was designed [98–101] [98–101] designed a nested ring gyroscope based on the single crystal. The structure of the gyroscope is a quality bonding pad on the outer ring, which could tune the frequency by means of filling solder leveling to offset the manufacture of frequency deviation. And the BI of the structure is 0.11 °/h. In the same year, T. H. Su *et al*. [102] used the EPI-Ploy process to manufacture a nested ring gyroscope with a central anchor point structure. Its quality factor is about 5×10^4 and its BI is 3.29 °/h. And D. Senkal *et al*. [103] used the epitaxial silicon encapsulation (EpiSeal) process to manufacture a nested ring gyroscope with a four-side anchor point structure, with a quality factor of up to 1×10^5 and a BI of 0.65 °/h.

On another hand, the researchers focused on different shapes of the nested ring gyroscope [104–110]. For example, the cobweb-like disk resonator gyroscope (DRG) is a duplication of the stiffness mass decoupled DRG reported in 2016 [107, 109], which for the first time provided a long-decay design method for the DRG. The design improves the performance because the decay time is the key to the stability of MEMS gyroscopes (in the case of no temperature control). The first BI of the stiffness mass decoupled DRG was 0.08 °/h [105] that was reported in 2018, which was further improved to 0.04 °/h [Fig. 8(b)] [106]. In 2018, B. Fan *et al*. reported a 16-face cobweb-like nested ring gyroscope, which consisted of 10 concentric 16-sided cobweb rings connected through 8 alternating spokes to a single central anchor [110]. After fabricated to silicon fusing bonded process and hermetically vacuum sealed by using a wafer-level packaging process, the frequency difference between the driving and sensing modes of the gyroscope is only 0.56 Hz, the quality factor is 1.13×10^5, the bias stability is 0.1 °/h, and the angle random walk reaches 0.005 °/h$^{1/2}$. In the same year, some researchers reported a new type of the nested ring gyroscope with the high immunity, which contributed to the mode-matching conditions [104]. The new structure no longer uses the nested ring structure, but a honeycomb-like disk structure. The model (left) and working modes (right) of the honeycomb disk resonator gyroscope (HDRG) are shown in Fig. 8(c). And the researchers described a high performance MEMS HDRG in 2021 with the BI of 0.015 °/h and 120 ppm in the range of ±300 °/s [111] and a rate-integrating HDRG with the 0.038 °/h BI and ±7000 °/s measurement range [112]. The design of the HDRG achieves stiffness-masses decoupling by hanging lumped-masses on the resonator. And the design could reach a much lower resonant frequency to get a higher thermoelastic quality factor and achieve the high quality factor of around 6×10^5. And the small size makes the transduction efficiency relatively low for an MEMS disk gyroscope with a very large capacitive area, which contributes to very low electronic noise. The stiffness-mass-decoupling strategy is employed to obtain the high stability. The bare honeycomb structure without stiffness-mass decoupling could only provide the BI of 8.9 °/h [108]. Exploiting the measurements of an HDRG, the researchers proposed a novel strategy for MEMS gyro-compassing in 2022, which greatly improved the compactness and reliability of north-finding systems and proved the possibility of eliminating the need for the physical rotation of MEMS gyroscopes [113].

Moreover, based on the MOEMS techniques, in 2020, D. Xia *et al*. [114–116] reported an electrostatically driven MEMS gyroscope with the nested ring structure and detected by the whispering gallery mode (WGM) mode, as shown in Fig. 8(d). It replaces the original capacitance sensing structure with the WGM resonator and measures the resonant wavelength shift due to the WGM cavity deformation. The obtained BI of this MOEMS gyroscope is 4.0399 °/h and the ARW is 0.4326 °/h$^{1/2}$.

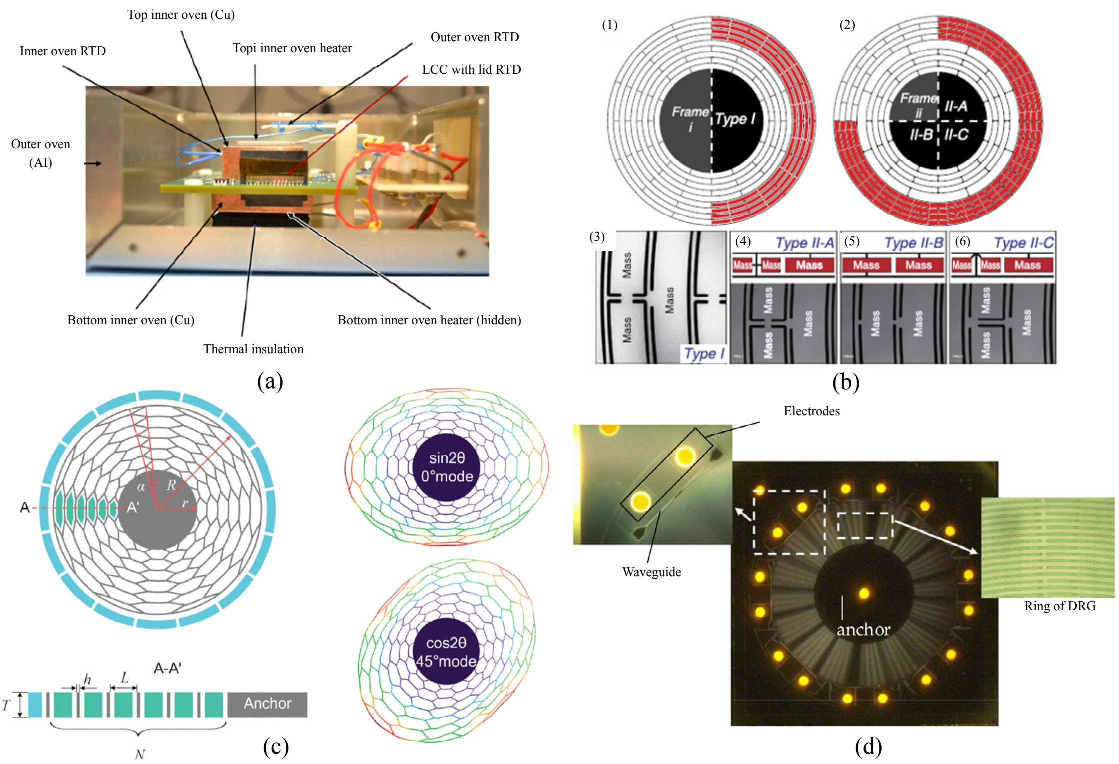

Fig. 8 Nested ring gyroscope [97, 106, 111, 114].

The nested ring gyroscope has the advantages of anti-interference and the high quality factor of both the vibratory ring gyroscope and hemispherical resonant gyroscope, and it is easy to be manufactured with the low cost. Therefore, it has a great potential for being a high-precision MEMS/MOEMS gyroscope. However, such a gyroscope still has some problems to be solved, such as the complex structure, too many parameters that should be optimized, difficult simulation, and difficult to analyze the noise performance from theoretical modeling.

3.4 Piezoelectric vibrating micro-gyroscope

The piezoelectric vibration micro-gyroscope can be divided into the piezoelectric ceramic vibration micro-gyroscope, solid acoustic micro-gyroscope, and quartz micro-gyroscope according to different materials, among which the solid acoustic micro-gyroscope can be further divided into the surface acoustic wave (SAW) micro-gyroscope and volume wave (BAW) micro-gyroscope. Compared with the traditional vibration micro-gyroscope, the piezoelectric vibration micro-gyroscope does not need to have the angular rate sensitive device and elastic structure of the whole movement, so it has strong impact resistance and vibration resistance, and does not need vacuum encapsulation.

Specifically, in 2006, K. Maenaka *et al.* [117] reported a new piezoelectric ceramic vibration micro-gyroscope, which consisted of a lead zirconate titanate prism with electrodes and a measurement and control circuit. It uses the inverse piezoelectric effect to excite the vibration and the piezoelectric effect to detect the angular rate signal. In 2009, Y. Lu *et al.* [118, 119] proposed a two-axis piezoelectric ceramic vibration micro-gyroscope with the high impact resistance, as shown in Fig. 9(a). The piezoelectric prism is still used as the main structure and the reference vibration frequency reaches 260 kHz.

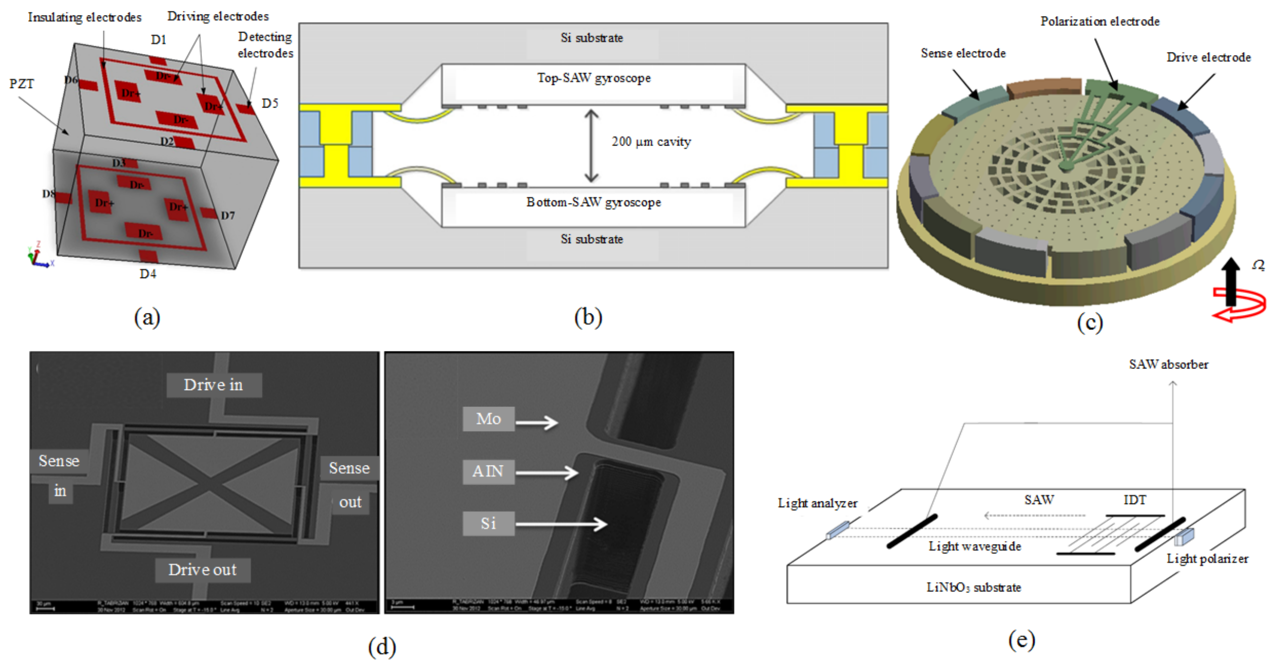

Fig. 9 Piezoelectric vibrating micro-gyroscope [118, 119, 125, 127–129].

The SAW micro-gyroscope also has no suspension structure, which has the advantages of the excellent shock resistance, wide dynamic range, and low power consumption. In 1997, M. Kurosawa *et al.* [120] produced the SAW gyroscope. Equal-spaced metal points are inserted in the middle of the double-ended SAW resonator, which excites SAW standing waves in the vertical direction. Then, in 1999, V. K. Varadan *et al.* [121–124] used this design idea to produce an SAW micro-gyroscope prototype using the standard IC process and obtained the 0.038 °/s/Hz$^{1/2}$ resolution. However, the output signal of the SAW micro-gyroscope based on the standing wave mode is too weak, which is hard to be used in practices. Moreover, the SAW micro-gyroscope based on the traveling wave mode has made considerable progress. In 2012, H. Oh *et al.* [125] produced a biaxial SAW micro-gyroscope in the traveling wave mode, which was composed of two layers of single-axis gyroscopes placed orthogonal. Figure 9(b) shows the micro-gyroscope structure [125]. The test results show that the sensitivity of the gyroscope is 0.907 Hz/°/s in the sense mode and 0.837 Hz/°/s in the drive mode.

The other kind of solid acoustic micro-gyroscope, the BAW gyroscope, is a new gyroscope developed in recent years. Its bulk sound wave is mainly generated by applying an alternating field on a piezoelectric single crystal sheet or piezoelectric film to stimulate fundamental or harmonic resonance along the thickness direction to obtain the high frequency bulk sound wave. In 2006, H. Johari *et al.* [126] used the HARPSS technology to manufacture the first BAW gyroscope on the SOI substrate. Its operating frequency is 5.9 MHz, the quality factor exceeds 2×10^6, and the measured sensitivity reaches 190 μV/°/s. In 2010 and 2013, the structures as shown in Figs. 9(c) and 9(d) were developed [127, 128], and their sensitivity reached 15 μV/°/s and 20.38 μV/°/s, respectively. The researchers reported a high-frequency resonant square micro-gyroscope using the piezoelectric transduction, which degenerated pairs of orthogonal flexural resonance modes to provide energy exchange paths in 2013.

Moreover, in 2010, S. X. Lu *et al.* [129] reported an MOMES gyroscope for extracting SAW gyroscopic effect signals using the Bragg diffraction of acoustic waves on light, as shown in Fig. 9(e). The method is to couple the rotational velocity information in the acoustic medium to the light and obtain the angular rate signal by measuring the change in the light intensity. The gyroscope has a sensitivity of 12 μV/°/s and a measurement range of 0–400 °/s.

3.5 Suspended rotor micro-gyroscope

Although the suspended rotor micro-gyroscope is manufactured based on the MEMS processing technology and packaged in chips for wider applications, the physical operating mechanism is still based on the angular momentum conservation rather than the Coriolis effect. Specifically, the suspended rotor micro-gyroscope can be divided into the electrostatic suspension and magnetic suspension. Maintaining the rotor at the zero-equilibrium position of the shell by the electromagnetic force and high speed rotation, the gyroscope measures the input angular rate with the help of the torque rebalancing principle.

In 2003, T. Murakoshi *et al.* reported the first electrostatic suspension five-axis rotor micro-gyroscope with closed-loop control. Using capacitive detection and electrostatic actuation achieves rotor levitation, and the rotation of the micro gyro is based on the principle of a planar variable capacitance motor. Its structure is shown in Fig. 10(a) [130], in which the ARW is 0.15 °/$h^{1/2}$. And an improvement in the performance was reported in 2005 [131] with the angle random walk of 0.085 °/$h^{1/2}$. Moreover, in 2012, T. Terasawa *et al.* used the pulse-width modulation (PWM) wave to realize electrostatic suspension, which was equipped with the full digital orthogonal frequency division multiplexing (OFDM) sensing technology to solve its multi-channel carrier [132]. The test results show that the ARW is 1.8 °/$h^{1/2}$. In 2012, F. T. Han *et al.* [133] from China also proposed an electrostatic suspension micro-gyroscope with a spin ring rotor, and the structure is shown in Fig. 10(b). Considering the actual negative spring effect in rotor dynamics, the dual-axis torque-rebalance loop is designed to investigate the loop stability and explain the experimental measurement. The BI is 50.95 °/h, and the ARW is 0.9 °/$h^{1/2}$.

The magnetic suspended rotor gyroscope was first proposed and produced by C. B. Williams *et al.* [134] in 1997. The experimental results show that the resolution of 24 °/$h^{1/2}$ could be obtained when the speed of rotation is 1 000 rpm. In 2006, W. Zhang *et al.* [135] from China proposed a gyroscope based on an alumina rotor with independent coils, whose prototype's scale factor was 0.212 V/°. There are eight pieces of the sector sense electrode and the rotor to construct a contactless capacitance displacement sense system. And it uses a four-phase induction micromotor to realize the rotor rotation. In 2009, G. Xue *et al.* [136] also proposed an inductor and capacitor (LC) tuned magnetic suspended rotor gyroscope and its structure is shown in Fig. 10(c). There was a 6-pole and 3-phase star, which has 6 coils surrounded by the 8-pole rotor. Whenever the rotor is displaced, a transformation of the difference between the upper electromagnet voltage and the under electromagnet voltage is measured. And the suspend rotor could spin at a high speed of 12 000 rpm.

By means of electrostatic suspension and magnetic suspension, the suspended rotor micro-gyroscopes eliminate the supporting shaft structure required by the traditional mechanical rotor gyroscope to greatly reduce the mechanical friction of the rotor and greatly improve the accuracy. Moreover, the floating rotor has a very high degree of freedom and can measure the three-axis acceleration and two-axis angular rate simultaneously, so it has a great advantage in the integration of the inertial measurement unit. However, the rotor micro-gyroscope is not widely used because of the difficulty of manufacturing, the high requirement of feedback control and tuning circuit, and the rotor heat deformation made by the eddy current effect.

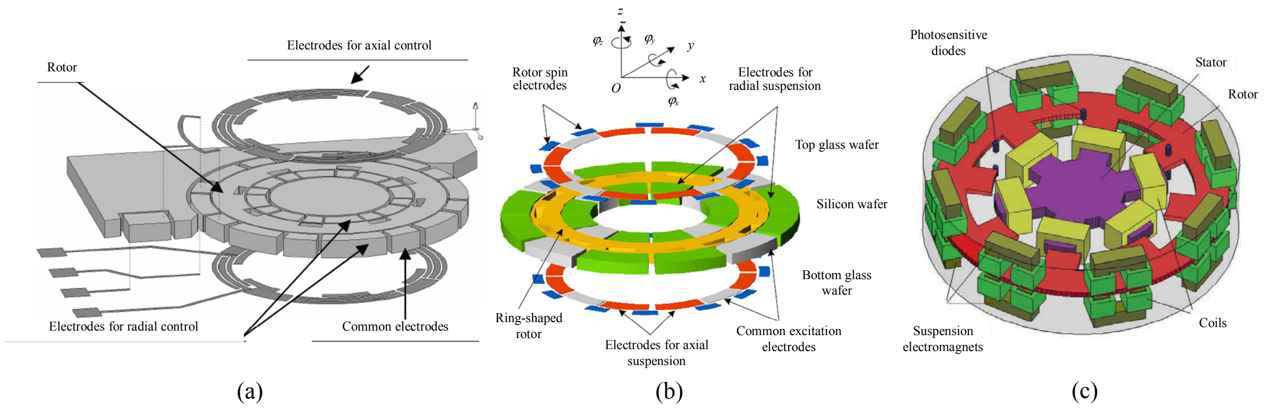

Fig. 10 Suspended rotor micro-gyroscope [130, 133, 136].

4. Research progress of MEMS/MOEMS gyroscope based Sagnac effect and nuclear magnetic resonance

4.1 Principle of traditional optical gyroscope

Regularly, optical gyroscopes use the Sagnac effect to measure the angular rate of rotation [137, 138]. As shown in Fig. 11, the dashed line and solid line are the paths taken by the beam traveling in the rotation direction and traveling against the rotation. When the circular optical path has a rotational angular rate relative to the inertial space, there is a difference between the direct and inverse optical paths, and the optical path difference ΔL is proportional to the angle θ. Therefore, the change in the angular rate can be obtained by measuring the change in the optical path difference.

Conventional optical gyroscopes can be divided into ring laser gyroscopes [137] and fiber optic gyroscopes [130] according to their Sagnac effect sensitive structures. The laser gyroscope is needed to make the gyroscope with its own inherent frequency jitter circuit do small angular vibration. If the gyroscope rotates, the fringe movement will be generated at the prism, and the angular position and angular rate signal of the gyroscope can be obtained by detecting and processing the fringe movement.

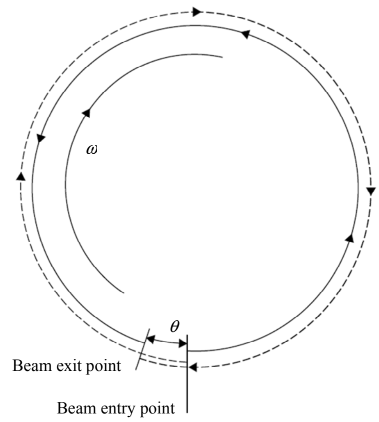

Fig. 11 Sagnac effect [167].

Another kind of optical gyroscope is the fiber optic gyroscope (FOG). According to its working principle, it can be divided into the interferometric fiber optic gyroscope (IFOG) [139], resonant fiber optic gyroscope (RFOG) [140], and Brillouin scattering fiber optic gyroscope (BFOG) [141], among which the interferometric fiber optic gyroscope technology is the most mature and widely used. The circular optical path required to produce the Sagnac effect is formed by the fiber loop wound by the n-loop fiber. The larger radius results in the longer total length of the fiber and the higher measurement accuracy of the gyroscope. Fiber optic gyroscopes manufactured by Honeywell are at the world's leading level [142]. This product is specially applied to the workspace and stable platform requiring long life and low noise and can work continuously for 15 years accurately with the BI between 0.002 °/h and 0.004 °/h and ARW of 0.003 °/$h^{1/2}$. The company's strategic grade interferometric fiber optic gyroscope products have the bias stability of 0.0002 °/h–0.0006 °/h. In 2013, the researchers from Stanford University demonstrated that by driving an FOG with a laser of relatively broad linewidth (10 MHz), the BI of the FOG is 1.1 °/s and the ARW is 0.058 °/$h^{1/2}$ [143].

Compared with the vibratory gyroscope, the optical gyroscope has no movable structure. Therefore, the advantages of the optical gyroscope include the long service life and strong anti-jamming capability. However, its large structure size and high cost make that its application in the field of the consumer electronics is restricted. So trying to use the MOEMS technology to reduce the volume of the optical gyroscope and production costs becomes the key research direction.

4.2 MOEMS optical gyroscope

Low light-level MOEMS optical gyroscopes can be divided into the resonant type and interference type. Specifically, resonant MOEMS optical gyroscopes are mainly realized by fabricating optical waveguide resonators on silicon wafers. Moreover, interferometric MOEMS optical gyroscopes replace optical fibers by means of the optical waveguide or micromirror array. Its working principle is the same as the traditional optical gyroscope, which uses the Sagnac effect to detect the angular velocity. It is an attempt to miniaturize the laser gyroscope and fiber optic gyroscope.

In 2000, the U.S. Air Force Institute of Technology [144] proposed an interferometric MOEMS gyroscope. As Fig. 12(a) shows, the gyroscope uses eight micro-mirrors manufactured by the MEMS technology to construct two optical loops over a small area to enhance the Sagnac effect. The gyroscope mainly focuses on the simulation and proof-of-concept stages, and the sensitivity of the prototype could reach 0.6761 °/s. In 2006, H. Liu *et al.* [145] reported another four-micromirror interferometric MOEMS gyroscope, as shown in Fig. 12(b). A spatial helical optical structure composed of micromirrors is designed. Light traveled in the free space, which could reduce wastage. Based on the theorem proving experiment, the Sagnac effect is proved and the BI of the gyroscope is 8 °/s [145]. And North University of China [146, 147] reported an MOMES gyroscope based on the planar micro-disk cavity and its planar micro-disk resonator structure in 2010. The laser is coupled to the micro-disk cavity through the Y-waveguide, traveling clockwise and counterclockwise, respectively, as shown in Fig. 12(c). The Sagnac effect is used to measure the angular rate. The diameter of the cavity is only 50 μm–60 μm, and the quality factor is 4.8×10^6. In 2012, W. Sa-Ngiamsak *et al.* [148] proposed a new MOMES gyroscope comprised of the modified add/drop filter known as the Panda ring resonator, where the optical path length had been enhanced utilizing the panda ring, as shown in Fig. 12(d). Simulation results show that phase difference as a function of the angular rate based on the Sagnac effect could be achieved. In 2016, the researchers [149] developed a new concept that double mirrors are used to reduce the influence of alignment errors, as shown in Fig. 12(e). By means of silicon direct bonding and consequently from 120° double mirrors, two similar structured wafers are connected. It allows the minimization of the influence of alignment errors by the use of double mirrors.

The Sagnac effect based optical gyroscopes have the good performance of the BI and ARW, but the large size and high cost of the traditional optical gyroscopes restrict the wide application. The MOEMS optical gyroscope uses the MEMS technology to process the key structure of the optical gyroscope, which not only retains the performance advantages of the optical gyroscope, but also reduces the cost and size. The key problem of the MOEMS optical gyroscope is how to design the optical resonator as long as possible with the high quality factor in the limited chip area to enhance the Sagnac effect. This technology route has become a research hotspot due to its potential for small size, low cost, and high precision.

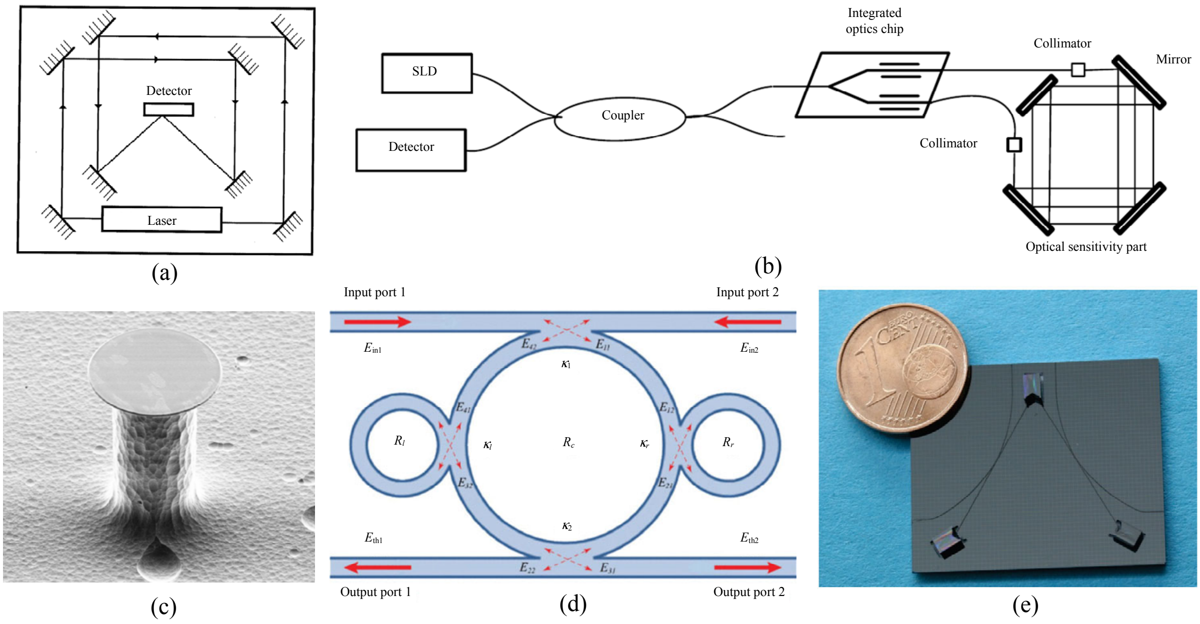

Fig. 12 MOEMS optical micro-gyroscope [144–149].

4.3 MEMS/MOEMS atomic gyroscope

The atomic gyroscope generates the specific spectral signal due to the external angular rate. It can be divided into two kinds of gyroscopes: atomic interference gyroscopes [150–158] based on the atomic interference using the Sagnac effect and nuclear magnetic resonance gyroscopes [159–166] based on the atomic spin effect. Both gyroscopes have a potential for achieving high precision and small size in theory.

The atomic interference gyroscope is a gyroscope based on the Sagnac effect of the matter wave. Since the length of the matter wave is 3×10^{4} times that of the visible light wave, according to the theoretical formula of the Sagnac effect, it can be concluded that the theoretical accuracy of the atomic interference gyroscope is 6×10^{10} times higher than that of the optical gyroscope. In 1997, Stanford University reported the atomic interference gyroscope based on the thermal atom beam and developed an atomic interferometer, which used two-photon velocity selective Roman transitions to keep atoms in ground states, as shown in Fig. 13(a). The short-term sensitivity of the atomic gyroscopes is as high as 2×10^{-8} rad/s/Hz$^{1/2}$ and has the promising potential for increasing the performance to 1×10^{-9} rad/s/Hz$^{1/2}$ by straightforward improvement [150]. They reported improvements to their atomic gyroscope in 2000, including the implementation of counterpropagating atomic beams and electronic rotation rate compensation to achieve a factor of 30 times increase in the short-term sensitivity to 6×10^{-10} rad/s/Hz^{1} [151], as shown in Fig. 13(b).

In 2020, Cornell University [152] reported the implementation method of a new atomic interference gyroscope for atom capture using the micro-nano optics technology, as shown in Fig. 13(c), with shot-noise limited rotation sensitivity of 0.0028 °/h$^{1/2}$. The development of the nuclear magnetic resonance (NMR) gyroscope is far better than the development of the atomic interference gyroscope. Detecting the atomic spin magnetic field outside the Larmor frequency shift to determine the angular rate without moving parts, is one of the developing directions of the next generation of the gyroscope.

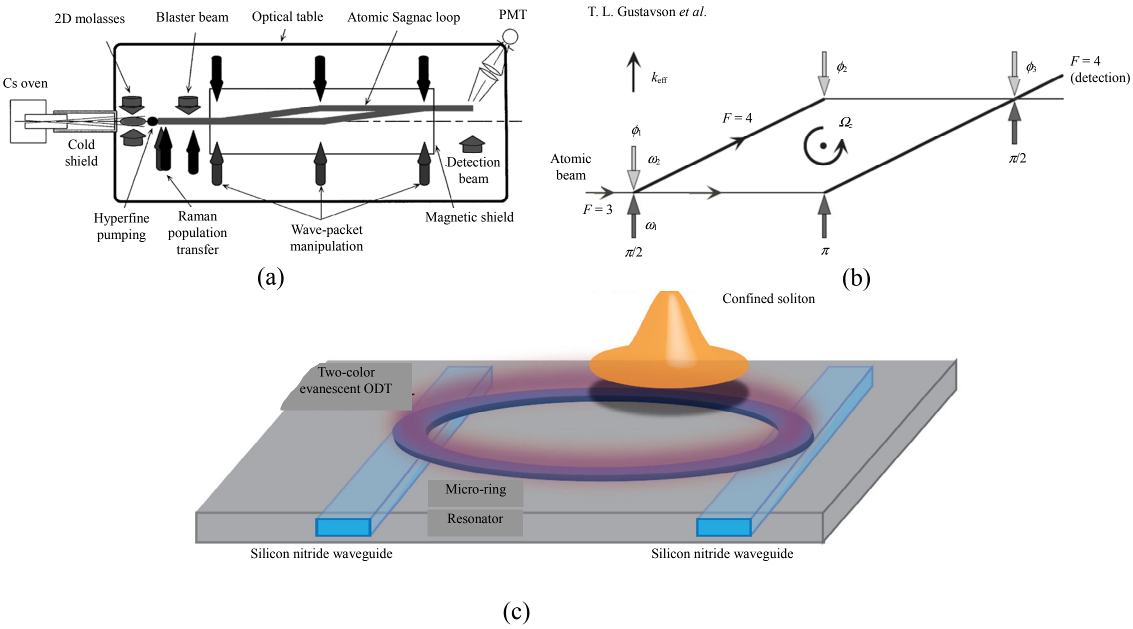

Fig. 13 MEMS/MOEMS atomic gyroscope [150–152].

The atomic laser gyroscope (ALG) based on the atomic chip may be the final direction of the cold atom gyroscope development [168]. The atomic chip is a device that integrates the electric field, magnetic field, and optical field on a small chip through the MOEMS technology to achieve cold atom trapping and control, and has the characteristics of miniaturization and high integration.

5. Conclusions and outlook

MEMS gyroscopes have developed rapidly since the first demonstration in 1988, showing the excellent performance. Moreover, MOEMS gyroscopes have the potential for achieving higher levels of performance by combining the advantages of the MEMS and optical sensing technologies. And the low cost, size, weight, and power (CSWaP) become the key points to enhance the competitiveness of inertial technology products. Defense Advanced Research Projects Agency (DARPA) proposed the CSWaP comprehensive index for inertial devices and systems, which is the product of cost, size, weight, and power consumption. In the review, the demands of applications and performance indexes for MEMS/MOEMS gyroscopes are analyzed and divided into several types in terms of the operation principle and structure, as listed in Table 2.

Due to the limitation of the MEMS/MOEMS fabrication accuracy and structural design, the performance of most micro-gyroscopes fails to reach the theoretical noise limit. Under the framework of the MEMS/MOEMS technology, the new generation of the gyroscope will make breakthroughs from two perspectives. On the one hand, we need to develop gyroscopes based on new working principles, such as nuclear magnetic resonance gyroscopes [166], cold atomic gyroscopes [168], cavity photomechanical gyroscopes [169–171], and quantum enhanced gyroscopes developed by using the modern quantum theory. The other is to improve the performance of the silicon micromechanical vibration gyroscope by improving the precision of the MEMS/MOEMS processing technology and designing the more reasonable driving structure, sensitive structure, and detection structure. The physical error of the MEMS gyroscopes is almost inversely proportional to the decaying time constant (inverse of the dissipation). It is important for high-performance gyroscopes to prolong the decaying time constant (or improve quality factor) [69, 76, 77, 78, 109]. And the compensation method of the multiple gyro system can also improve the accuracy. For example, in the MEMS inertial measurement unit (IMU), a multi-axis MEMS gyro redundant configuration is adopted to improve the performance through mutual calibration of a set of gyroscopes in the same direction. However, the gyroscope is adjusted at the expense of bandwidth and dynamics to achieve the satisfactory precision. For example, some researchers reported that the MEMS IMU provided an excellent precision of better than 0.02 °/h with the BI of 0.006 °/h and ARW of around 0.003 $°/h^{1/2}$ [172].

Table 2 Typical specifications of various MEMS/MOMES gyroscopes along with their characteristics and applications.

Parameter	Coriolis force				Angular momentum	Sagnac effect		
	Frame	Ring	Hemispherical resonant	Piezoelectric vibrating	Suspended rotor	Traditional optical	MOMES optical	Atomic
BI(°/h)	>0.100	>0.010	<0.500	>0.100	>0.100	<0.150	>0.100	<0.010
ARW($°/h^{1/2}$)	>0.050	>0.005	<0.100	>0.050	>0.010	<0.050	>0.100	<0.001
Characteristics	Simple configuration, small, and low cost	Strong resistance and low cost	Strong resistance and high sensitivity	Strong resistance and simple package	High degree and multi-axis	High sensitivity and large	Small, low cost, and high sensitivity	Ultra-high sensitivity
Main applications	Consumer electronics and automobile	Automobile and aerial vehicle	Aerospace, ship, and ammunition	Aerospace and aerial vehicle	Aerospace and ship	Aerospace, ship, and ammunition	Research stage	Research stage

As mentioned above, new principles, structures, and processes are constantly updated and developed to achieve higher performances. Inertia technologies are driven by high performance, low cost, high reliability, small size, weight, and integrated systems. In different application scenarios, this review believes that there are two directions for the further development. On the one hand, the performance limit of the traditional gyroscope is broken through the principle innovation and special material innovation. On the other hand, the further improvements in matching circuits, error correction, and temperature control achieve high performance and low cost in highly integrated IMUs.

Acknowledgment

This work was supported in part by the National Natural Science Foundation of China (Grant Nos. U2230206, 12074058, 62371106, and 61971113), the National Key Research and Development Program for Young Scientists (Grant No. 2022YFA1405900), the Joint Fund of Ministry of Education (Grant No. 8091B022126), the Fundamental Enhancement Program Technology Area Fund (Grant No. 2021-JCJQ-JJ-0667), and Sichuan Provincial Science and Technology Planning Program of China (Grant Nos. 2021YJ0089, 2022YFG0230, and 2023YFG0040).

Declarations

Conflict of Interest The authors declare that they have no competing interests.

References

[1] M. N. Armenise, C. Ciminelli, F. Dell'Olio, and V. M. N. Passaor, "*Advances in Gyroscope Technologies*," Berlin: Springer, 2010.

[2] V. Passaro, A. Cuccovillo, L. Vaiani, M. De Carlo, and C. Campanella, "Gyroscope technology and applications: a review in the industrial perspective," *Sensors*, 2017, 17(10): 2284.

[3] I. A. Faisal, T. W. Purboyo, and A. S. R. Ansori, "A review of accelerometer sensor and gyroscope sensor in IMU sensors on motion capture," *Journal of Engineering and Applied Sciences*, 2019, 15(3): 826–829.

[4] A. Jarmola, S. Lourette, V. M. Acosta, A. G. Birdwell, P. Blumler, D. Budker, *et al*., "Demonstration of diamond nuclear spin gyroscope," *Science Advances*, 2021, 7(43): ebal3840.

[5] V. V. Soshenko, V. S. Bolshedvorskii, O. Rubinas, V. N. Sorokin, A. N. Smolyaninov, V. V. Vorobyov, *et al*., "Nuclear spin gyroscope based on the nitrogen vacancy center in diamond," *Physical Review Letters*, 2021, 126(19): 197702.

[6] K. Liu, W. Zhang, W. Chen, K. Li, F. Dai, F. Cui, *et al*., "The development of micro-gyroscope technology," *Journal of Micromechanics and Microengineering*, 2009, 19(11): 113001.

[7] D. Xia, C. Yu, and L. Kong, "The development of micromachined gyroscope structure and circuitry technology," *Sensors*, 2014, 14(1): 1394–1473.

[8] Z. Guo, F. Cheng, B. Li, L. Cao, C. Lu, and K. Song, "Research development of silicon MEMS gyroscopes: a review," *Microsystem Technologies*, 2015, 21: 2053–2066.

[9] X. Ren, X. Zhou, S. Yu, X. Wu, and D. Xiao, "Frequency-modulated MEMS gyroscopes: a review," *IEEE Sensors Journal*, 2021, 21(23): 26426–26446.

[10] B. Boxenhorn and P. Greiff, "A vibratory micromechanical gyroscope," in *Guidance, Navigation and Control Conference*, Minneapolis, 1988, pp. 15–17.

[11] T. K. Tang, R. C. Gutierrez, C. B. Stell, V. Vorperian, G. A. Arakaki, J. T. Rice, *et al*., "A packaged silicon MEMS vibratory gyroscope for microspacecraft," in *Proceedings IEEE The Tenth Annual International Workshop on Micro Electro Mechanical Systems. An Investigation of Micro Structures, Sensors, Actuators, Machines and Robots*, Nagoya, 1997, pp. 26–30.

[12] K. Larkin, M. Ghommem, M. Serrano, and A. Abdelkefi, "A review on vibrating beam-based micro/nano-gyroscopes," *Microsystem Technologies*, 2021, 27: 4157–4181.

[13] M. Y. Fan and L. F. Zhang, "Research progress of quartz tuning fork micromachined gyroscope," in *2015 International Conference on Artificial Intelligence and Industrial Engineering*, Phuket, 2015, pp. 26–27.

[14] Z. Qin, Y. Gao, J. Jia, X. Ding, L. Huang, and H. Li, "The effect of the anisotropy of single crystal silicon on the frequency split of vibrating ring gyroscopes," *Micromachines*, 2019, 10(2): 126.

[15] J. Jia, X. Ding, Z. Qin, Z. Ruan, W. Li, X. Liu, *et al.*, "Overview and analysis of MEMS Coriolis vibratory ring gyroscope," *Measurement*, 2021, 182: 109704.

[16] N. Yazdi, F. Ayazi, and K. Najafi, "Micromachined inertial sensors," *Proceedings of the IEEE*, 1998, 86(8): 1640–1659.

[17] J. Gholinejad and K. Abedi, "Design and analysis of a MOEMS gyroscope based on a ring-shaped hybrid structure," *Plasmonics*, 2023, 18: 1159–1172.

[18] M. Hodjat-Shamami and F. Ayazi, "Eigenmode operation of piezoelectric resonant gyroscopes," *Microsystems & Nanoengineering*, 2020, 6(1): 108.

[19] N. C. Tsai, J. S. Liou, C. C. Lin, and T. Li, "Suppression of dynamic offset of electromagnetic drive module for micro-gyroscope," *Mechanical Systems and Signal Processing*, 2011, 25(2): 680–693.

[20] Y. Chen, E. E. Aktakka, J. K. Woo, K. Najafi, and K. R. Oldham, "On-chip capacitive sensing and tilting motion estimation of a micro-stage for in situ MEMS gyroscope calibration," *Mechatronics*, 2018, 56: 242–253.

[21] S. Rahmanian, S. Hosseini-Hashemi, and M. Rezaei, "Out-of-plane motion sensing in encapsulated electrostatic MEMS gyroscopes: principal parametric resonance," *International Journal of Mechanical Sciences*, 2021, 190: 106022.

[22] Y. Wang, R. Cao, C. Li, and R. N. Dean, "Concepts, roadmaps and challenges of ovenized MEMS gyroscopes: a review," *IEEE Sensors Journal*, 2020, 21(1): 92–119.

[23] M. Li, X. Ding, and S. Qin, "Design of a novel lower-noise tunneling magnetoresistance micromachined gyroscope," *Microsystem Technologies*, 2019, 25: 1447–1454.

[24] H. Cao, Y. Liu, Z. Kou, Y. Zhang, X. Shao, J. Gao, *et al*., "Design, fabrication and experiment of double U-beam MEMS vibration ring gyroscope," *Micromachines*, 2019, 10(3): 186.

[25] M. Ren, H. Xu, X. Han, C. Dong, and X. Lu, "Low noise interface ASIC of micro gyroscope with ball-disc rotor," *Sensors*, 2020, 20(4): 1238.

[26] W. Wang, T. Zhang, D. Fan, and C. Xing, "Study on frequency stability of a linear-vibration MEMS gyroscope," *Microsystem Technologies*, 2014, 20(12): 2147–2155.

[27] M. Hosseini-Pishrobat and J. Keighobadi, "Robust vibration control and angular velocity estimation of a single-axis MEMS gyroscope using perturbation compensation," *Journal of Intelligent & Robotic Systems*, 2019, 94(1): 61–79.

[28] P. Greiff, B. Boxenhorn, T. King, and L. Niles,

"Silicon monolithic micromechanical gyroscope," in *1991 International Conference on Solid-State Sensors and Actuators. Digest of Technical Papers*, San Francisco, 1991, pp. 24–27.

[29] S. E. Alper and T. Akin, "A planar gyroscope using a standard surface micromachining process," in *The 14th European Conference on Solid-State Transducers (Eurosensors XIV)*, Kobenhavn, 2000, pp. 27–30.

[30] K. Maenaka, S. Ioku, N. Sawai, T. Fujita, and Y. Takayama, "Design, fabrication and operation of MEMS gimbal gyroscope," *Sensors & Actuators A: Physical*, 2005,121(1): 6–15.

[31] M. Norgia and S. Donati, "Hybrid opto-mechanical gyroscope with injection-interferometer readout," *Electronics Letters*, 2001, 37(12): 756–758.

[32] A. Sheikhaleh, K. Jafari, and K. Abedi, "Design and analysis of a novel MOEMS gyroscope using an electrostatic comb-drive actuator and an optical sensing system," *IEEE Sensors Journal*, 2018, 19(1): 144–150.

[33] C. Trigona, B. Andò, and S. Baglio, "Development of integrated vibratory-gyroscopes based on photonic bandgap materials," in *2015 IEEE Metrology for Aerospace (MetroAeroSpace)*, Benevento, 2015, pp. 114–117.

[34] C. Trigona, B. Andò, and S. Baglio, "Fabrication and characterization of an MOEMS gyroscope based on photonic bandgap materials," *IEEE Transactions on Instrumentation and Measurement*, 2016, 65(12): 2840–2852.

[35] M. Li, X. Ding, and S. Qin, "Design of a novel lower-noise tunneling magnetoresistance micromachined gyroscope," *Microsystem Technologies*, 2019, 25: 1447–1454.

[36] M. Li, Z. Wang, H. Geng, Q. Wu, R. Zhang, Z. Cui, *et al*., "Structural design and simulation of a micro-gyroscope based on nano-grating sensing," *Microsystem Technologies*, 2019, 25: 1627–1637.

[37] K. Xie, R. Zhang, C. Xin, L. Jin, Z. Wang, Z. Wang, *et al*., "Micro-opto-electro-mechanical gyroscope based on the Talbot effect of a single-layer near-field diffraction grating," *Applied Optics*, 2021, 60(13): 3724–3731.

[38] X. Zhao, B. Zhou, R. Zhang, and Z. Chen, "Research on laser trimming of silicon MEMS vibratory gyroscopes," *Integrated Ferroelectrics*, 2011, 129(1): 37–44.

[39] X. S. Liu, Z. C. Yang, X. Z. Chi, J. Cui, H. T. Ding, Z. Y. Guo, *et al*., "A doubly decoupled lateral axis micromachined gyroscope," *Sensors and Actuators A: Physical*, 2009, 154(2): 218–223.

[40] X. Liang, S. Gao, F. Gao, and S. Lv, "Design and simulation of a micro gyroscope with decoupled and high linearity structure," in *The 9th International Conference on Electronic Measurement & Instruments*, Beijing, 2009, pp. 16–19.

[41] J. Xie, Q. Shen, Y. Hao, H. Chang, and W. Yuan, "Design, fabrication, and characterization of a low-noise *z*-axis micromachined gyroscope," *Microsystem Technologies*, 2015, 21: 625–630.

[42] J. Bernstein, S. Cho, T. A. King, A. Kourepenis, P. Maciel, and M. Weinberg, "A micromachined comb-drive tuning fork rate gyroscope," in *Proceedings IEEE Micro Electro Mechanical Systems*, Fort Lauderdale, 1993, pp. 143–148.

[43] M. Lutz, W. Golderer, J. Gerstenmeier, J. Marek, B. Maihofer, S. Mahler, *et al*., "A precision yaw rate sensor in silicon micromachining," in *Proceedings of International Solid State Sensors and Actuators Conference*, Chicago, 1997, pp. 847–850.

[44] A. Sharma, M. F. Zaman, V. B. Amini, and F. Ayazi, "A high-*Q* in-plane SOI tuning fork gyroscope," in *Sensors, 2004 IEEE*, Vienna, 2004, pp. 24–27.

[45] M. F. Zaman, A. Sharma, and F. Ayazi, "High performance matched-mode tuning fork gyroscope," in *The 19th IEEE International Conference on Micro Electro Mechanical Systems*, Istanbul, 2006, pp. 22–26.

[46] Z. Hao, M. F. Zaman, A. Sharma, and F. Ayazi, "Energy loss mechanisms in a bulk-micromachined tuning fork gyroscope," in *Sensors, 2006 IEEE*, Daegu, 2006, pp. 22–25.

[47] L. Cao, J. Li, X. Liu, and F. Sun. "Research on an anchor point lever beam coupling type tuning fork micro-gyroscope," *International Journal of Precision Engineering and Manufacturing*, 2020, 21: 1099–1111.

[48] A. Sharma, M. F. Zaman, and F. Ayazi, "A sub-0.2 °/hr bias drift micromechanical silicon gyroscope with automatic CMOS mode-matching," *IEEE Journal of Solid-State Circuits*, 2009, 44(5): 1593–1608.

[49] A. Sharma, M. F. Zaman, M. Zucher, and F. Ayazi, "A 0.1°/HR bias drift electronically matched tuning fork microgyroscope," in *2008 IEEE 21st International Conference on Micro Electro Mechanical Systems*, Tucson, 2008, pp. 13–17.

[50] A. A. Trusov, A. R. Schofield, and A. M. Shkel, "Gyroscope architecture with structurally forced anti-phase drive-mode and linearly coupled anti-phase sense-mode," in *TRANSDUCERS 2009 – 2009 International Solid-State Sensors, Actuators and Microsystems Conference*, Denver, 2009, pp. 21–25.

[51] A. A. Trusov, I. P. Prikhodko, S. A. Zotov, and A. M. Shkel, "Low dissipation silicon tuning fork gyroscopes for rate and whole angle measurements," *IEEE Sensors Journal*, 2011, 11(11): 2763–2770.

[52] Y. J. Cho, "High-Performance micromachined vibratory rate and rate-integrating gyroscopes," Ph.D. dissertation, University of Michigan, USA, 2012.

[53] M. S. Weinberg and A. Kourepenis, "Error sources in in-plane silicon tuning-fork MEMS gyroscopes,"

Journal of Microelectromechanical Systems, 2006, 15(3): 479–491.
[54] L. Huang, Y. Ni, and Y. Yin, "Fabrication error analysis on dual-mass silicon micro-gyroscope," in *2011 International Conference on Electrical and Control Engineering*, Yichang, 2011, pp. 16–18.
[55] Y. Guan, S. Gao, L. Jin, and L. Cao, "Design and vibration sensitivity of a MEMS tuning fork gyroscope with anchored coupling mechanism," *Microsystem Technologies*, 2016, 22: 247–254.
[56] Y. Chen, J. Jiao, B. Xiong, L. Che, X. Li, and Y. Wang, "A novel tuning fork gyroscope with high *Q*-factors working at atmospheric pressure," *Microsystem Technologies*, 2005, 11: 111–116.
[57] L. Che, B. Xiong, Y. Li, and Y. Wang, "A novel electrostatic-driven tuning fork micromachined gyroscope with a bar structure operating at atmospheric pressure," *Journal of Micromechanics and Microengineering*, 2009, 20(1): 015025.
[58] J. Zhou, T. Jiang, J. Jiao, and M. Wu, "Design and fabrication of a micromachined gyroscope with high shock resistance," *Microsystem Technologies*, 2014, 20: 137–144.
[59] Z. Y. Guo, Z. C. Yang, Q. C. Zhao, L. T. Lin, H. T. Ding, X. S. Liu, *et al*., "A lateral-axis micromachined tuning fork gyroscope with torsional *Z*-sensing and electrostatic force-balanced driving," *Journal of Micromechanics and Microengineering*, 2009, 20(2): 025007.
[60] Z. Y. Guo, Z. C. Yang, L. T. Lin, Q. C. Zhao, J. Cui, X. Z. Chi, *et al*., "A lateral-axis micromachined tuning fork gyroscope with novel driving and sensing combs," in *TRANSDUCERS 2009 – 2009 International Solid-State Sensors, Actuators and Microsystems Conference*, Denver, 2009, pp. 288–291.
[61] Z. Y. Guo, L. T. Lin, Q. C. Zhao, Z. C. Yang, H. Xie, G. Z. Yan, *et al*., "A lateral-axis microelectromechanical tuning-fork gyroscope with decoupled comb drive operating at atmospheric pressure," *Journal of Microelectromechanical Systems*, 2010, 19(3): 458–468.
[62] Z. Y. Guo, Z. C. Yang, L. T. Lin, Q. C. Zhao, J. Cui, X. Z. Chi, *et al*., "Decoupled comb capacitors for microelectromechanical tuning-fork gyroscopes," *IEEE Electron Device Letters*, 2009, 31(1): 26–28.
[63] C. He, Q. Zhao, J. Cui, Z. Yang, and G. Yan, "A research of the bandwidth of a mode-matching MEMS vibratory gyroscope," in *The 7th IEEE International Conference on Nano/Micro Engineered and Molecular Systems (NEMS)*, Kyoto, 2012, pp. 738–741.
[64] H. Cao and H. Li, "Investigation of a vacuum packaged MEMS gyroscope architecture's temperature robustness," *International Journal of Applied Electromagnetics and Mechanics*, 2013, 41(4): 495–506.
[65] B. Yang, X. Wang, D. Hu, and L. Wu, "Research on the non-ideal dynamics of a dual-mass silicon micro-gyroscope," *Microsystem Technologies*, 2017, 23: 151–162.
[66] B. Yang, X. Wang, Y. Deng, and D. Wu, "Mechanical coupling error suppression technology for an improved decoupled dual-mass micro-gyroscope," *Sensors*, 2016, 16(4): 503.
[67] T. Zhang, B. Zhou, P. Yin, Z. Chen, and R. Zhang, "Optimal design of a center support quadruple mass gyroscope (CSQMG)," *Sensors*, 2016, 16(5): 613.
[68] B. Zhou, T. Zhang, P. Yin, Z. Chen, M. Song, and R. Zhang, "Innovation of flat gyro: center support quadruple mass gyroscope," in *2016 IEEE International Symposium on Inertial Sensors and Systems*, Laguna Beach, 2016, pp. 42–45.
[69] A. A. Trusov, G. Atikyan, D. M. Rozelle, A. D. Meyer, S. A. Zotov, B. R. Simon, *et al*., "Flat is not dead: current and future performance of Si-MEMS quad mass gyro (QMG) system," in *2014 IEEE/ION Position, Location and Navigation Symposium – PLANS 2014*, Monterey, 2014, pp. 252–258.
[70] D. Endean, K. Christ, P. Duffy, E. Freeman, M. Glenn, M. Gnerlich, *et al*., "Near-navigation grade tuning fork MEMS gyroscope," in *2019 IEEE International Symposium on Inertial Sensors and Systems (INERTIAL)*, Naples, 2019, pp. 1–4.
[71] J. Cho, S. Singh, T. Nagourney, J. K. Woo, A. Darvishian, B. Shiari, *et al*., "High-*Q* navigation-grade fused-silica micro birdbath resonator gyroscope," in *Sensors, 2021 IEEE*, Sydney, 2021, pp. 1–4.
[72] J. Y. Cho and K. Najafi, "A high-*Q* all-fused silica solid-stem wineglass hemispherical resonator formed using micro blow torching and welding," in *The 28th IEEE International Conference on Micro Electro Mechanical Systems (MEMS)*, Estoril, 2015, pp. 18–22.
[73] T. Nagourney, J. Y. Cho, B. Shiari, A. Darvishian, and K. Najafi, "259 second ring-down time and 4.45 million quality factor in 5.5 kHz fused silica birdbath shell resonator," in *the 19th International Conference on Solid-State Sensors, Actuators and Microsystems (TRANSDUCERS)*, Kaohsiung, 2017, pp. 18–22.
[74] S. Singh, J. K. Woo, G. He, J. Y. Cdsho, and K. Najafi, "0.0062 $^\circ/\sqrt{\text{hr}}$ angle random walk and 0.027 °/hr bias instability from a micro-shell resonator gyroscope with surface electrodes," in *2020 IEEE 33rd International Conference on Micro Electro Mechanical Systems (MEMS)*, Vancouver, 2020, pp. 18–22.
[75] M. J. Ahamed, D. Senkal, and A. M. Shkel, "Effect of annealing on mechanical quality factor of fused quartz hemispherical resonator," in *2014 International Symposium on Inertial Sensors and*

Systems (ISISS), Laguna Beach, 2014, pp. 1–4.

[76] D. Senkal, M. J. Ahamed, M. H. A. Ardakani, S. Askari, and A. M. Shkel, "Demonstration of 1 million *Q*-factor on microglassblown wineglass resonators with out-of-plane electrostatic transduction," *Journal of Microelectromechanical Systems*, 2015, 24(1): 29–37.

[77] J. Y. Cho, S. Singh, J. K. Woo, G. He, and K. Najafi, "0.00016 deg/$\sqrt{\text{hr}}$ angle random walk (ARW) and 0.0014 deg/hr bias instability (BI) from a 5.2M-Q and 1-cm precision shell integrating (PSI) gyroscope," in *2020 IEEE International Symposium on Inertial Sensors and Systems (INERTIAL)*, Hiroshima, 2020, pp. 23–26.

[78] J. Cho, S. Singh, T. Nagourney, J. K. Woo, A. Darvishian, B. Shiari, *et al.*, "High-*Q* navigation-grade fused-silica micro birdbath resonator gyroscope," in *Sensors, 2021 IEEE*, Sydney, 2021, pp. 1–4.

[79] K. Lu, W. Li, Z. Hou, D. Xiao, Y. Wu, X. Wu, *et al.*, "Effective mechanical trimming of micro shell resonator with T-shape masses," in *The 19th International Conference on Solid-State Sensors, Actuators and Microsystems (TRANSDUCERS)*, Kaohsiung, 2017, pp. 18–22.

[80] Y. Chen, X. Xi, Y. Shi, K. Lu, D. Xiao, and X. Wu, "Simulated prediction of structural asymmetry for glass blown micro shell resonators," in *2020 IEEE International Symposium on Inertial Sensors and Systems (INERTIAL)*, Hiroshima, 2020, pp. 23–26.

[81] D. Xiao, W. Li, Z. Hou, K. Lu, Y. Shi, Y. Wu, *et al.*, "Fused silica micro shell resonator with T-shape masses for gyroscopic application," *Journal of Microelectromechanical Systems*, 2017, 27(1): 47–58.

[82] Y. Shi, K. Lu, X. Xi, Y. Wu, D. Xiao, and X. Wu, "Geometric imperfection characterization and precise assembly of micro shell resonators," *Journal of Microelectromechanical Systems*, 2020, 29(4): 480–489.

[83] X. Lu, X. Xi, K. Lu, C. Wang, X. Chen, Y. Wu, *et al.*, "Miniature ultralight deformable squama mechanics and skin based on piezoelectric actuation," *Micromachines*, 2021, 12(8): 969.

[84] K. Lu, X. Xi, W. Li, Y. Shi, Z. Hou, M. Zhuo, *et al.*, "Research on precise mechanical trimming of a micro shell resonator with T-shape masses using femtosecond laser ablation," *Sensors and Actuators A: Physical*, 2019, 290: 228–238.

[85] W. Li, X. Xi, K. Lu, Y. Shi, Z. Hou, Y. Wu, *et al.*, "A novel high transduction efficiency micro shell resonator gyroscope with 16 T-shape masses using out-of-plane electrodes," *IEEE Sensors Journal*, 2019, 19(13): 4820–4828.

[86] Y. Shi, K. Lu, B. Li, Y. Chen, X. Xi, Y. Wu, *et al.*, "Ultrafast laser in fabrication of micro hemispherical resonators with quality factor over millions," *Journal of Micromechanics and Microengineering*, 2021, 31(5): 055002.

[87] M. W. Putty, "A micromachined vibrating ring gyroscope," Ph.D. dissertation, University of Michigan, Ann Arbor, USA, 1995.

[88] F. Ayazi and K. Najafi, "Design and fabrication of high-performance polysilicon vibrating ring gyroscope," in *Proceedings MEMS 98. IEEE. Eleventh Annual International Workshop on Micro Electro Mechanical Systems. An Investigation of Micro Structures, Sensors, Actuators, Machines and Systems*, Heidelberg, 1998, pp. 25–29.

[89] F. Ayazi and K. Najafi, "A HARPSS polysilicon vibrating ring gyroscope," *Journal of Microelectrochemical Systems*, 2001, 10(2): 169–179.

[90] G. He and K. Najafi, "A single-crystal silicon vibrating ring gyroscope," in *The Fifteenth IEEE International Conference on Micro Electro Mechanical Systems*, Las Vegas, 2002, pp. 718–721.

[91] F. M. Zaman, A. Sharma, and F. Ayazi, "The resonating star gyroscope: a novel multiple-shell silicon gyroscope with sub-5 deg/hr allan deviation bias instability," *IEEE Sensors Journal*, 2009, 9(6): 616–624.

[92] D. Chen, M. Zhang, and J. Wang, "An electrostatically actuated micromachined vibrating ring gyroscope with highly symmetric support beams," in *Sensors, 2010 IEEE*, Waikoloa, 2010, pp. 860–863.

[93] S. Yoon, U. Park, J. Rhim, and S. S. Yang, "Tactical grade MEMS vibrating ring gyroscope with high shock reliability," *Microelectronic Engineering*, 2015, 142: 22–29.

[94] Z. Li, S. Gao, L. Jin, H. Liu, and S. Niu, "Micromachined vibrating ring gyroscope architecture with high-linearity, low quadrature error and improved mode ordering," *Sensors*, 2020, 20(15): 4327.

[95] D. Keymeulen, C. Peay, D. Foor, T. Trung, A. Bakhshi, P. Withington, *et al.*, "Control of MEMS disc resonance gyroscope (DRG) using a FPGA platform," in *2008 IEEE Aerospace Conference*, Big Sky, 2008, pp. 1–8.

[96] A. D. Challoner, H. H. Ge, and J. Y. Liu, "Boeing disc resonator gyroscope," in *2014 IEEE/ION Position, Location and Navigation Symposium – PLANS 2014*, Monterey, 2014, pp. 504–514.

[97] R. L. Kubena, R. J. Joyce, and A. D. Challoner, "Correlation of frequency, temperature, and bias stability of a Si ring gyro," in *2016 IEEE International Symposium on Inertial Sensors and Systems*, Laguna Beach, 2016, pp. 22–25.

[98] D. Schwartz, D. J. Kim, and R. T. M'Closkey, "Frequency tuning of a disk resonator gyro via mass matrix perturbation," in *2008 American Control Conference*, Seattle, 2008, pp. 11–13.

[99] D. Schwartz, D. Kim, and R. M'Closkey, "A model-based approach to multi-modal mass tuning of a micro-scale resonator," in *2012 American Control Conference (ACC)*, Montreal, 2012, pp. 27–29.

[100] D. Schwartz and R. T. M'Closkey, "Decoupling of a disk resonator from linear acceleration via mass matrix perturbation," *Journal of Dynamic Systems Measurement & Control*, 2012, 134(2): 021005.

[101] D. Kim and R. M'Closkey, "A MEM vibratory gyro with mode-matching achieved by resonator mass loading," in *2014 IEEE/ION Position, Location and Navigation Symposium – PLANS 2014*, Monterey, 2014, pp. 499–503.

[102] T. H. Su, S. H. Nitzan, P. Taheri-Tehrani, M. H. Kline, B. E. Boser, and D. A. Horsley, "Silicon MEMS disk resonator gyroscope with an integrated CMOS analog front-end," *IEEE Sensors Journal*, 2014, 14(10): 3426–3432.

[103] D. Senkal, S. Askari, M. J. Ahamed, E. J. Ng, V. Hong, Y. Yang, *et al*., "100K *Q*-factor toroidal ring gyroscope implemented in wafer-level epitaxial silicon encapsulation process," in *2014 IEEE 27th International Conference on Micro Electro Mechanical Systems (MEMS)*, San Francisco, 2014, pp. 26–30.

[104] Q. Li, D. Xiao, X. Zhou, Z. Hou, Y. Xu, Q. Hu, *et al*., "Research on the high fabrication error immunity of the honeycomb-like disk resonator gyroscope," in *2018 IEEE Micro Electro Mechanical Systems (MEMS)*, Belfast, 2018, pp. 21–25.

[105] X. Zhou, D. Xiao, Q. Li, Z. Hou, K. He, Z. Chen, *et al*., "Decaying time constant enhanced MEMS disk resonator for high precision gyroscopic application," *IEEE/ASME Transactions on Mechatronics*, 2018, 23(1): 452–458.

[106] Q. Li, D. Xiao, X. Zhou, Y. Xu, M. Zhuo, Z. Hou, *et al*., "0.04 degree-per-hour MEMS disk resonator gyroscope with high-quality factor (510 k) and long decaying time constant (74.9 s)," *Microsyst Nanoeng*, 2018, 4(1): 32.

[107] X. Zhou, D. Xiao, X. Wu, Y. Wu, Z. Hou, K. He, *et al*., "Stiffness-mass decoupled silicon disk resonator for high resolution gyroscopic application with long decay time constant (8.695 s)," *Applied Physics Letters*, 2016, 109(26): 263501.

[108] Q. Li, D. Xiao, X. Zhou, Z. Hou, Y. Xu, Q. Hu, *et al*., "Research on the high fabrication error immunity of the honeycomb-like disk resonator gyroscope," in *2018 IEEE Micro Electro Mechanical Systems (MEMS)*, Belfast, 2018, pp. 1016–1019.

[109] X. Zhou, D. Xiao, X. Wu, Q. Li, Z. Hou, K. He, *et al.*, "Mitigating thermoelastic dissipation of flexural micromechanical resonators by decoupling resonant frequency from thermal relaxation rate," *Physical Review Applied*, 2017, 8(6): 064033.

[110] B. Fan, S. Guo, L. Yu, M. Cheng, M. Zhou, W. Hu, *et al*., "A novel sixteen-sided cobweb-like disk resonator gyroscope with low as-fabricated frequency split between drive and sense modes," in *Sensors, 2018 IEEE*, New Delhi, 2018, pp. 28–31.

[111] Y. Xu, Q. Li, P. Wang, Y. Zhang, X. Zhou, L. Yu, *et al*., "0.015 degree-per-hour honeycomb disk resonator gyroscope," *IEEE Sensors Journal*, 2021, 21(6): 7326–7338.

[112] Y. Zhang, S. Yu, J. Sun, K. Lu, Y. Xu, Q. Li, *et al.*, "A rate-integrating honeycomb disk resonator gyroscope with 0.038 °/h bias instability and ±7 000 °/s measurement range," *IEEE Electron Device Letters*, 2021, 42(4): 581–584.

[113] T. Miao, Q. Li, X. Hu, X. Wu, W. Wu, and D. Xiao, "Virtual rotating MEMS gyrocompassing with honeycomb disk resonator gyroscope," *IEEE Electron Device Letters*, 2022, 43(8): 1331–1334.

[114] X. Shen, L. Zhao, and D. Xia, "Research on the disc sensitive structure of a micro optoelectromechanical system (MOEMS) resonator gyroscope," *Micromachines*, 2019, 10(4): 264.

[115] D. Xia, L. Huang, and L. Zhao, "A new design of an MOEMS gyroscope based on a WGM microdisk resonator," *Sensors*, 2019, 19(12): 2798.

[116] D. Xia, B. Zhang, H. Wu, and T. Wu, "Optimization and fabrication of an MOEMS gyroscope based on a WGM resonator," *Sensors*, 2020, 20(24): 7264.

[117] K. Maenaka, H. Kohara, M. Nishimura, T. Fujita, and Y. Takayama, "Novel solid micro-gyroscope," in *The 19th IEEE International Conference on Micro Electro Mechanical Systems*, Istanbul, 2006, pp. 22–26.

[118] Y. Lu, W. Zhang, X. Wu, W. Chen, and F. Cui, "Design and analysis of novel solid biaxial micro-gyroscope with special mode excitation," in *The 4th IEEE International Conference on Nano/Micro Engineered and Molecular Systems*, Shenzhen, 2009, pp. 291–294.

[119] Y. Lu, X. Wu, W. Zhang, W. Chen, F. Cui, and W. Liu, "Research on reference vibration for a two-axis piezoelectric micro-machined gyroscope," *Journal of Micromechanics & Microengineering*, 2010, 20(7): 075039.

[120] M. Kurosawa, Y. Fukuda, M. Takasaki, and T. Higuchi, "A surface-acoustic-wave gyro sensor," *Sensors and Actuators A: Physical*, 1997, 66(1–3): 33–39.

[121] V. K. Varadan and V. V. Varadan, "MEMS-IDT-based microaccelerometers and gyroscopes," *Electronics and Structures for MEMS. SPIE*, 1999, 3891: 134–143.

[122] V. K. Varadan, W. D. Suh, P. B. Xavier, K. A. Jose, and V. V. Varadan, "Design and development of a MEMS-IDT gyroscope," *Smart Materials and Structures*, 2000, 9(6): 898.

[123] V. K. Varadan, K. A. Jose, P. B. Xavier, D. Suh, and V. V. Varadan, "Conformal MEMS-IDT gyroscopes and their comparison with fiber optic gyro," *Smart Structures and Materials 2000: Smart Electronics and MEMS. SPIE*, 2000, 3999: 335–344.

[124] V. K. Varadan, W. D. Suh, K. A. Jose, and V. V. Varadan, "Hybrid MEMS-IDT-based accelerometer and gyroscope in a single chip," *Smart Structures and Materials 2001: Smart Electronics and MEMS. SPIE*, 2001, 4334: 119–128.

[125] H. Oh, K. J. Lee, S. S. Yang, and K. Lee, "Development of novel dual-axis sensing gyroscope using surface acoustic wave," *Microelectronic Engineering*, 2012, 97(6): 259–264.

[126] H. Johari and F. Ayazi, "Capacitive bulk acoustic wave silicon disk gyroscopes," in *2006 International Electron Devices Meeting*, San Francisco, 2006, pp. 11–13.

[127] W. K. Sung, M. Dalal, and F. Ayazi, "A 3 MHz spoke gyroscope with wide bandwidth and large dynamic range," in *2010 IEEE 23rd International Conference on Micro Electro Mechanical Systems (MEMS)*, Hong Kong, 2010, pp. 24–28.

[128] R. Tabrizian, M. Hodjat-Shamami, and F. Ayazi, "High-frequency AlN-on-silicon resonant square gyroscopes," *Journal of Microelectromechanical Systems*, 2013, 22(5): 1007–1009.

[129] S. X. Lu, S. F. Chen, and Y. Zhao, "MOEMS gyroscope based on acoustooptic mode coupling," in *Asia Communications and Photonics Conference and Exhibition. Optica Publishing Group*, Shanghai, 2010, pp. 799001.

[130] T. Murakoshi, Y. Endo, K. Fukatsu, S. Nakamura, and M. Esashi, "Electrostatically levitated ring-shaped rotational-gyro/accelerometer," *Japanese Journal of Applied Physics*, 2003, 42(4S): 2468.

[131] S. Nakamura, "MEMS inertial sensor toward higher accuracy & multi-axis sensing," in *Sensors, 2005 IEEE*, Irvine, 2005, pp. 4.

[132] T. Terasawa, T. Watanabe, and T. Murakoshi, "Electrostatically levitated ring-shaped rotational-gyro/accelerometer using all-digital OFDM detection with TAD," in *Sensors, 2012 IEEE*, Taipei, 2012, pp. 1–4.

[133] F. T. Han, Y. F. Liu, L. Wang, and G. Y. Ma, "Micromachined electrostatically suspended gyroscope with a spinning ring-shaped rotor," *Journal of Micromechanics & Microengineering*, 2012, 22(10): 105032.

[134] C. B. Williams, C. Shearwood, P. H. Mellor, and R. B. Yates, "Modelling and testing of a frictionless levitated micromotor," *Sensors & Actuators A: Physical*, 1997, 61(1–3): 469–473.

[135] W. Zhang, W. Chen, X, Zhao, X. Wu, W. Liu, X. Huang, *et al.*, "The study of an electromagnetic levitating micromotor for application in a rotating gyroscope," *Sensors and Actuators A: Physical*, 2006, 132(2): 651–657.

[136] G. Xue, X. Zhang, and H. Zhang, "Electromagnetic design of a magnetically suspended gyroscope prototype," in *2009 International Conference on Applied Superconductivity and Electromagnetic Devices*, Chengdu, 2009, pp. 369–372.

[137] W. W. Chow, J. Gea-Banacloche, L. M. Pedrotti, V. E. Sanders, W. Schleich, and M. O. Scully, "The ring laser gyro," *Reviews of Modern Physics*, 1985, 57(1): 61.

[138] V. Vali and R. W. Shorthill, "Fiber ring interferometer," *Applied Optics*, 1976, 15(5): 1099–1100.

[139] H. C. Lefère, "Fundamentals of the interferometric fiber-optic gyroscope," *Optical Review*, 1997, 4(1A): 20–27.

[140] M. A. Terrel, M. J. F. Digonnet, and S. Fan, "Resonant fiber optic gyroscope using an air-core fiber," *Journal of Lightwave Technology*, 2011, 30(7): 931–937.

[141] F. Zarinetchi, S. P. Smith, and S. Ezekiel, "Stimulated Brillouin fiber-optic laser gyroscope," *Optics Letters*, 1991, 16(4): 229–231.

[142] T. Shiozawa, V. T. Dau, D. V. Dao, H. Kumagai, and S. Sugiyama, "A dual axis thermal convective silicon gyroscope," in *Micro-Nanomechatronics and Human Science*, *2004 and The Fourth Symposium Micro-Nanomechatronics for Information-Based Society*, Nagoya, 2004, pp. 277–282.

[143] S. W. Lloyd, S. Fan, and M. J. F. Digonnet, "Experimental observation of low noise and low drift in a laser-driven fiber optic gyroscope," *Journal of Lightwave Technology*, 2013, 31(13): 2079–2085.

[144] J. P. Stringer, "The air force institute of technology (AFIT) micro electro-mechanical systems (MEMS) interferometric gyroscope (MiG)," M.S. thesis, Air Force Institute of Technology, Wright Patterson AFB, USA, 2000.

[145] H. Liu, L. Feng, H. Lin, and C. Zhang, "Research on a novel MOEMS interferometric gyroscope," *Sixth International Symposium on Instrumentation and Control Technology: Sensors, Automatic Measurement, Control, and Computer Simulation. SPIE*, 2006, 6358: 178–182.

[146] M. Zhao, S. Yan, Y. Yan, P. Jia, Z. Liu, J. Li, *et al.*, "Investigation and analysis of a MOEMS gyroscope based on novel resonator," in *2010 Academic Symposium on Optoelectronics and Microelectronics Technology and 10th Chinese-Russian Symposium on Laser Physics and Laser Technology Optoelectronics Technology (ASOT)*, Harbin, 2010, pp. 337–340.

[147] J. Liu, X. Wang, M. Zhao, Y. Yan, P. Jia, Y. Zhang, *et al.*, "The research of a novel gyroscope based on

high *Q* micro-resonator," in *The 6th IEEE International Conference on Nano/Micro Engineered and Molecular Systems*, Kaohsiung, 2011, pp. 1132–1135.

[148] W. Sa-Ngiamsak, C. Sirawattananon, K. Srinuanjan, S. Mitatha, and P. P. Yupapin, "Micro-optical gyroscope using a PANDA ring resonator," *IEEE Sensors Journal*, 2012, 12(8): 2609–2613.

[149] T. Niesel and A. Dietzel, "Micro-clamps for precise positioning of 120° silicon double mirrors in a MOEMS gyroscope," *Microelectronic Engineering,* 2016, 159: 27–31.

[150] T. L. Gustavson, P. Bouyer, and M. A. Kasevich, "Precision rotation measurements with an atom interferometer gyroscope," *Physical Review Letters*, 1997, 78(11): 2046–2049.

[151] T. L. Gustavson, A. Landragin, and M. A. Kasevich, "Rotation sensing with a dual atom-interferometer Sagnac gyroscope," *Classical and Quantum Gravity*, 2000, 17(12): 2385.

[152] Y. S. Patil, H. F. H. Cheung, S. A. Bhave, and M. Vengalattore, "System design of a cold atom gyroscope based on interfering matter-wave solitons," in *2020 IEEE International Symposium on Inertial Sensors and Systems (INERTIAL)*, Hiroshima, 2020, pp. 23–26.

[153] B. Canuel, F. Leduc, D. Holleville, A. Gauguet, J. Fils, A. Virdis, *et al*., "Six-axis inertial sensor using cold-atom interferometry," *Physical Review Letters*, 2006, 97(1): 010402.

[154] B. Dubetsky and M. A. Kasevich, "Atom interferometer as a selective sensor of rotation or gravity," *Physical Review A*, 2006, 74(2): 023615.

[155] L. A. Sidorenkov, R. Gautier, M. Altorio, R. Geiger, and A. Landragin, "Tailoring multiloop atom interferometers with adjustable momentum transfer," *Physical Review Letters*, 2020, 125(21): 213201.

[156] J. K. Stockton, K. Takase, and M. A. Kasevich, "Absolute geodetic rotation measurement using atom interferometry," *Physical Review Letters*, 2011, 107(13): 133001.

[157] I. Dutta, D. Savoie, B. Fang, B. Venon, C. L. G. Alzar, R. Geiger, *et al*., "Continuous cold-atom inertial sensor with 1 nrad/sec rotation stability," *Physical Review Letters*, 2016, 116(18): 183003.

[158] D. Savoie, M, Altorio, B. Fang, L. A. Sidorenkov, R. Geiger, and A. Landragin, "Interleaved atom interferometry for high-sensitivity inertial measurements," *Science Advances*, 2018, 4(12): eaau7948.

[159] Q. Shu, F. Ji, and M. Zhu, "Analysis and demonstration of the in-situ magnetometer for nuclear magnetic resonance gyroscopes," *Journal of Magnetic Resonance*, 2022, 335: 107128.

[160] D. Meyer and M. Larsen, "Nuclear magnetic resonance gyro for inertial navigation," *Gyroscopy and Navigation*, 2014, 5(2): 75–82.

[161] J. Qin, S. Wang, F. Gao, Y. Wang, and W. Han, "Advances in nuclear magnetic resonance gyroscope," *Navigation Positioning Timing*, 2014, 1: 64–69.

[162] E. A. Donley. "Nuclear magnetic resonance gyroscopes," in *Sensors, 2010 IEEE*, Waikoloa, 2010, pp. 17–22.

[163] M. Larsen and M. Bulatowicz. "Nuclear magnetic resonance gyroscope: for DARPA's micro-technology for positioning, navigation and timing program," in *IEEE International Frequency Control Symposium Proceedings*, Baltimore, 2012, pp. 21–24.

[164] K. F. Woodman, P. W. Franks, and M. D. Richards, "The nuclear magnetic resonance gyroscope: a review," *The Journal of Navigation*, 1987, 40(3): 366–384.

[165] R. M. Noor and A. M. Shkel, "MEMS components for NMR atomic sensors," *Journal of Microelectromechanical Systems*, 2018, 27(6): 1148–1159.

[166] L. Jiang, W. Quan, R. Li, W. Fan, F. Liu, J. Qin, *et al*., "A parametrically modulated dual-axis atomic spin gyroscope," *Applied Physics Letters*, 2018, 112(5): 054103.

[167] O. J. Woodman, "An introduction to inertial navigation," Ph.D. dissertation, University of Cambridge, Cambridge, UK, 2007.

[168] R. FolMan, P. Krüger, D. Cassettari, B. Hessmo, T. Maier, and J. Schmiedmayer, "Controling cold atoms using nanofabricated surfaces: atom chips," *Physical Review Letters*, 2000, 84(20): 4749–4752.

[169] S. Davuluri, K. Li, and Y. Li, "Gyroscope with two-dimensional optomechanical mirror," *New Journal of Physics*, 2017, 19(11): 113004.

[170] K. Li, S. Davuluri, and Y, Li, "Improving optomechanical gyroscopes by coherent quantum noise cancellation processing," *Science China Physics Mechanics & Astronomy*, 2018, 61: 1–7.

[171] G. Li, X. Lu, X. Wang, J. Xin, and X. Li, "Optomechanical gyroscope simultaneously estimating the position of the rotation axis," *Journal of the Optical Society of America B*, 2022, 39(1): 98–106.

[172] W. Zhao, Y. Cheng, S. Zhao, X. Hu, Y. Rong, J. Duan, *et al*., "Navigation grade MEMS IMU for a satellite," *Micromachines*, 2021, 12(2): 151.